MODELING AND SIMULATION OF GAS RELEASE FROM RUPTURE OF SUBSEA SURFACE GAS PIPE

A DISSERTATION

Submitted in partial fulfillment of the

requirements for the award of the degree of

MASTER OF TECHNOLOGY

In

CHEMICAL ENGINEERING

(With specialization in Industrial Safety and Hazard Management)

BY

ANKITA GUPTA

DEPARTMENT OF CHEMICAL ENGINEERING

INDIAN INSTITUTE OF TECHNOLOGY, ROORKEE

ROORKEE-247667 (INDIA)

JUNE 2014

DECLARATION

I hereby declare that the work being presented in the seminar report entitled "MODELING AND SIMULATION OF GAS RELEASE FROM RUPTURE OF SUBSEA SURFACE GAS PIPE" in partial fulfillment of the requirements for the award of the degree of Master of Technology with specialization in Industrial Safety and Hazard Management and submitted in the Department of Chemical Engineering of the Indian Institute of Technology Roorkee, Roorkee, is an authentic record of my own work carried out during the period from May 2013 to June 2014 under the supervision of Prof. I.M. Mishra, Department of Chemical Engineering, Indian Institute of Technology Roorkee, Roorkee, India. The matter presented in this report has not been submitted by me for the award of any other degree of this or any other institute.

Place: Roorkee **Ankita Gupta**

Date: Enrolment. No.12516001

CERTIFICATE

This is to certify that the above statement made by the candidate is correct to the best of my knowledge.

(Dr. I.M. Mishra)

Professor

Department of Chemical Engineering,

Indian Institute of Technology Roorkee

ACKNOWLEDGEMENT

I wish to express my sincere gratitude and appreciations to Prof. I. M. Mishra, Department of Chemical Engineering, Indian Institute of Technology Roorkee, Roorkee for providing me an opportunity to work under his guidance. Their superb guidance with enriched knowledge, regular encouragement and valuable suggestions at every stage of the present work has proved to be extremely beneficial to me. I consider myself fortunate to have had the opportunity to work under their able guidance and enrich myself from their depths of knowledge.

I would also like to thank to Dr. V.K. Agarwal, Professor and Head, Department of Chemical Engineering, Indian Institute of Technology Roorkee, Roorkee for his continuous support during the M.tech. programme and extend my gratitude to Dr. Vimal singh and Dr. V.C. Srivastav who helped me with their valuable suggestions and assistance at every stage to finish my work.

I express my sincere thanks to R/S Jyoti Sharma, Nilamber Bariha, Partha Kundu, Praveen Kumar for their support which helped me directly or indirectly, in completion of work.

Ankita Gupta

Enrollment No. : 12516001

Indian Institute of Technology Roorkee

#

Abstract

There are several pipelines which are lying underwater for transportation of gases and other hydrocarbons. These pipelines may get damaged due to several accidents, that results in release of gas which rises as a plume and affects free surface. Risk assessments for offshore installations involve the modeling of the consequences of a range of accident scenarios. This may include the release of hydrocarbon inventory from top sides process equipment, subsea pipelines or risers or blowout events. Release from risers, subsea pipelines and subsea blowouts will result in dispersion of the hydrocarbon as it rises to the sea surface. This report presents a review of current status of the modeling of subsea gas releases and assesses the implication of using the modeling within a risk assessment.

Type of modeling available for subsea gas dispersion ranges from simple empirical approximation to integral or CFD computer programs. A survey of operators showed that it was the former empirical approximations which tended to be used within risk assessment studies, due to their ease of use for large number of cases, although CFD has been used in a research context. In all cases, lack of full scale data meant that the models have not been validated for the high release rates common for rupture of subsea pipelines.

Here we studied about release of LNG from pipe and variation of properties along the depth of sea. Plume structure and time taken by plume to reach surface has been noticed. Effect of water current on plume is also studied. When LNG is released in water, it suddenly vaporizes, which results in increase of temperature but it gets decrease along the path and with the time. Effect of gas concentration on marine animals is studied.

Table of content

List of Tables

List of Figures

Nomenclature

Symbol	Description
p	Pressure of gas
V_g	Volume of gas
y(t)	Dimensionless displacement
P(z)	Pressure at height z above sea bed
P(o)	Pressure at source
b	Radius or sub sea plume
w	Centerline velocity
H	Depth of release
g	Acceleration due to gravity
V_o	Volumetric flow rate
k	Fluid turbulent kinetic energy
U(r, z)	Local vertical fluid velocity
F_r	Froude number
U(z)	Centerline plume velocity as a function of depth z
U_b	Bubble slip velocity
S(z)	Density defect along plume centerline
m_f	Mass flux of plume at surface
Mp	Momentum flux of plume at surface
U_Φ	Velocity vector for phase Φ

$S_{F\Phi}$	Source term for phase in transport equations
r_{Φ}	Volume fraction of phase within plume
$T_{f\Phi}$	Diffusion coefficient for phase
F_D	Drag force exerted on bubble
d_b	Bubble diameter
C_d	Bubble drag coefficient
P_b	Turbulent kinetic energy
Eo	Eotvos number
x_i	Direaction vector
U_i	Mean velocity
S_0	Area of orifice
Y	Dimensionless expansion factor
p_a	Pressure at station a
p_b	Pressure at station b
u_j	Jet outflow velocity
v_j	Volumetric flow rate
d_j	Jet diameter
S_j	Vertical distance where jet completely breaks down
d_p	Maximum diameter of liquid droplet
d_j'	Effective diameter of jet
Bo_j	Jet Bond Number
Re_j	Reynold number
We_j	Jet Weber number
Lp_j	Weber-Reynold number
U_d	Liquid droplet rise velocity

K	Mass transfer coefficient
n	Number of moles of gas bubbles
A	Surface area of gas bubble
C_o	Concentration of dissolved gas
C_s	Saturated value of concentration
H	Henry constant
$\mathbf{x}^{1}$	Mole fraction of dissolved gas
f^g	Fugacity of gas in gas phase
R	Universal gas constant
v^{1}	Partial molar volume of gas
D	Molecular diffusivity of gas in liquid
d_e	Equilibrium diameter of bubble

Greek symbols

Symbols	**Description**
ρ_w	Density of water
ρ_g	Density of gas
ρ_L	Density of liquid
γ	Specific heat ratio
υ_w	Kinematic viscosity
β	Ratio of orifice diameter to pipe
σ_j	Surface tension of jet
λ	Heat of vaporization

Chapter 1
Introduction

1.1 General Introduction

Liquefied natural gas or LNG is basically the natural gas which predominantly contains methane, CH_4 that has been converted to liquid state or phase so that it can be easily for stored and transported. Natural gas is cooled to produce LNG and is cooled up to -162^0C which then gets liquefied, reducing its volume by a factor of more than 600. LNG is colorless, nontoxic, non-corrosive gas. If LNG is leaked into air or water, it warms up and a rapid increase in gaseous volume takes place which results in a gaseous/vapor cloud that can be flammable. If vapor cloud is lighter than air, it will rise and travel downwind. When NG/LNG is transported through sub-sea pipe lines, the pipe line and its accessories encounter huge hydrostatic pressure of sea water and corrosive environment of the sea, the tidal waves and the adhesion growth of sea-lives including barnacles. Under the prevailing temperature and pressure, there is a probability of leakage of the LNG/NG at the pipeline level. The leaked liquid gets converted into gaseous form due to pressure reduction, and the heating due to warmer sea water, and the gas will rise up due to buoyancy and get released from the sea surface.

Safety is the heart of all operations in oil and gas industry. Subsea release of gas due to rupture poses a threat to operational safety, and safety assets integrity for third parties which are operating offshore. On increasing the number of sub-sea installations and pipelines, the risk of potential faults is also increasing simultaneously. Several incidents which have occurred in the past due to sub-sea gas releases have illustrated the need for improved knowledge about the behaviour and risk of hydrocarbon release and emissions under water. Underwater explosion effects have also been the subject of extensive study by a number of investigators.

The analysis of the consequences of hydrocarbon release involve several stages: from release rate and associated depressurization calculations, through the modeling of liquid spread and gas dispersion, to the assessment of the fire and explosion and their potential for escalation.

In order to understand the consequences and the effects of underwater gas release, there is a need to make risk abatement strategies. It is also important to note the quantitative impact of gas release due to pipeline failure. Release from the subsea pipeline results in the dispersion of hydrocarbons as the release plume rises to the sea surface. The effects of a subsea release as the hydrocarbon plume reaches the surface will depend on a number of factors, and is also dependent on whether the release is in gaseous or liquid. If the release is in liquid phase, the buoyancy will result in the spreading of the liquid (lighter than water) on water surface. This spreading will form either a polluting slick, or if ignited due to an ignition source it will form an expanding pool fire. In the case of gas release, although the buoyancy is rather much larger than that for liquid release, the drag forces will cause the plume to break up between the point of release and the sea-surface, and rise the released gas will rise to the surface as a series of gaseous bubbles.

1.2 Pipeline Incidents

A number of incidents involving hydrocarbon leakage from pipelines have been recorded in recent years. Pipe line incidents are shown in the table:

Table 1: Some case studies of sub-sea gas pipeline leaks. (SINTEF, 2009)

Date	**Incident**	**Water Depth**	**Remarks**
April 29, 2001	Texaco Exploration and Production Pipeline segment no. 10393 South Marsh Island, Block 236	4.26 m	An incoming 0.0508 m gas lift line was ruptured. The break caused damage to the upper work deck, handrails, flow line, and riser. Personnel working on an adjacent well heard the bleeding gas, reported the incident to Texaco personnel who immediately shut-off the supply of gas to the line. No injuries or pollution were reported.
January 3 2002	Chevron USA Inc. Pipeline segment no. 13154		During an ESD (Emergency Shut Down), the 10-inch incoming shutdown valve closed, but the safety system on the platform failed to

	West Cameron, Block 48	6.70 m	operate. Shortly after, the platform operators noticed gas bubbles in the water approximately 91 m from the platform. The pipeline, which was 37 years old, was allowed to bleed for 90 minutes, and was later found to have ruptured at three places.
January 15, 2002	Transcontinental Gas Pipeline Company Pipeline segment no. 1526 Vermillion, block 67	12 m	The operator at an adjacent platform reported a pipeline rupture from 0.406 m diameter with a fire on the water. The pipeline was shut down and the fire ceased. No injuries or pollution were reported.
November 2009	Gas transmission pipeline, Ohio.		A 1.066 m transmission gas pipeline, failed on second day of operation. There was no fire but evacuation resulted.
April 2012	North Sea		The leak of flammable gas was discovered during operations to kill a well and quickly prompted the evacuation of all 238 workers aboard the Elgin drilling platform about 250 miles east of Aberdeen, Scotland.
December 2012	Florida gas transmission company	6.09 m	A rupture was detected, and no fire and injury was detected.
February 19, 2013	Fibre-optic cable company, in Kansas.		An independent contractor installing fiber-optic cable for a cable company in Kansas City, Missouri inadvertently struck an underground gas line on February 19. Gas later caught fire, and created an explosion that destroyed a popular local restaurant, killing one of the

			workers there, and injuring about 15 others near the scene
February, 13, 2014	Columbia Gulf Gas Transmission Pipeline		A 0.762 m Columbia Gulf Transmission gas pipeline carrying natural gas exploded near Knifley, Kentucky on February 13, sending two people to the hospital with injuries

How to detect natural gas leakage

To detect a pipeline leakage is by eyes, ears and nose. **Look** – Discoloring of vegetation and persistent bubbling in standing water are possible signs of leak around the pipeline area. On ground a liquid pool is formed with a dense white cloud or fog, a light mist of ice; or a frozen cloud is found near the pipeline.

Listen – on leakage it sounds noise like a hissing or roaring.

Smell – an unusual and strange odour which is like smell of rotten eggs, and petroleum

Some gases are odorless, and odorant as an additive cannot always be added. It is also important to notice your eyes and eyes as well as your nose to recognize a potential problem.

1.3 Liquefied Natural Gas

The LNG supply chain consists of 4 interlinked and independently-operated parts: exploration of gas from its sources and then production, liquefying a gas, shipping, as well as re-gasified, stored and distributed. The following flow diagram illustrate the production, conditioning of NG/LNG and transportation of LNG.

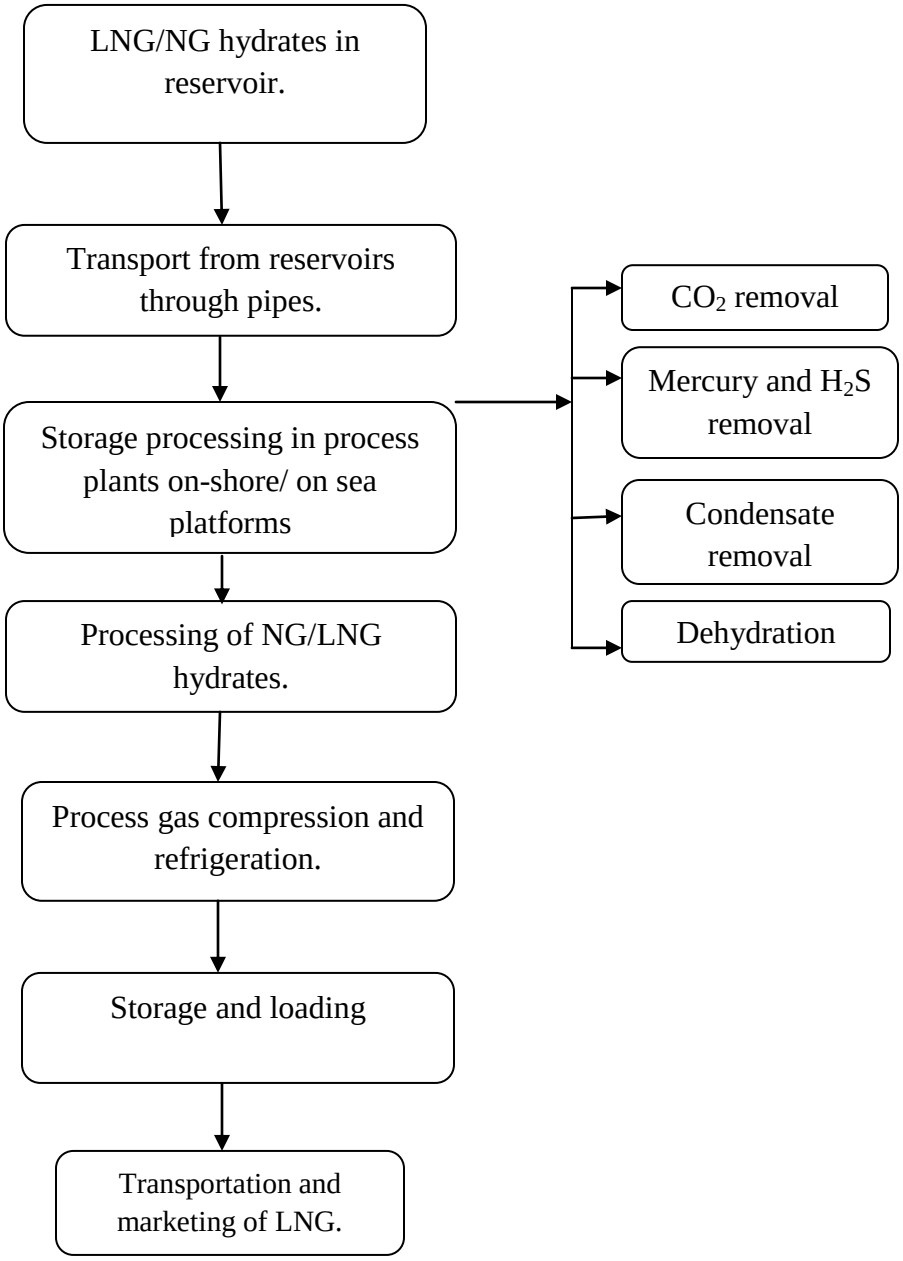

Fig 1.1 Flow diagram for the processing and transportation of natural gas in the form of LNG.

A typical LNG process is shown in figure, the gas is first extracted from well is transported to a processing plant where it is further purified by removing impurities and condensate such as water, oil, mud, as well as other gases such as CO_2 and H_2S. An especially designed LNG process train will also be used to remove trace amounts of mercury from the gas to prevent amalgamizing of mercury with aluminium in the cryogenic heat exchangers. This gas is then cooled down to cryogenic temperature of about -162^0 C under atmospheric pressure in steps until it gets completely liquefied. LNG is finally stored in storage tanks and are loaded and shipped to onshore terminals. At most of the onshore terminals, the LNG is transferred to insulated storage tanks designed to specifically hold LNG. These storage tanks can be either above or below the ground and are built to keep the liquid at a low temperature to minimize evaporation. Methane is a major constituent of LNG, typically about 90 % is methane. It also contains some other hydrocarbons and other gases like ethane, hydrogen sulfide and carbon-di-oxide.

When natural gas is needed, the LNG is warmed (using a regasification process involving heat exchangers) until it converts back to its gaseous state.

Table 2: Properties of LNG

Composition	Mainly composed of methane (85% to 94%), other hydrocarbons like ethane, propane, butane. Nitrogen, hydrogen sulphide and carbon dioxide are present in traces, but they are removed during NG to LNG processing.
Density	0.42 kg/l to 0.47 kg/l. In some cases it may high as 0.52 kg/l.
Temperature	Boiling temperature range is -166^0C to -57^0C
Viscosity	10^{-4} Pa.s to $2x10^{-4}$ Pa.s
Molecular weight (μ)	17 kmol/kg
Critical Temperature T_c	190.6 K
Critical Pressure P_c	$4.64x10^6$ Pa
Atmospheric boiling temperature T_b	111.6 K

Freezing temperature T_f	91.0 K
Liquid density at boiling point (for pure methane) ρ_L	422.6 kg/m^3
Liquid density at boiling point (commercial LNG) ρ_L	450 kg/m^3
Vapor density at boiling point ρ_v	1.82 kg/m^3
Density of gas at NTP, $\rho_{v, NTP}$	0.667 kg/m^3
Heat of vaporization (λ)	510 kJ/kg
Specific heat of vapor at constant pressure Cp	2200 J/kg K
Ratio of specific heat (γ)	1.30815
LFL in air	5%
UFL in air	15%
Specific gravity (liquid) at -162 ^{0}C	0.415-0.45
Surface tension (liquid) at -162 ^{0}C	0.014 N/m

1.3.1 Transportation of LNG

Natural gas is projected to be the fastest growing major fuel source through 2030 because it is cleaner-burning, reliable and abundant. Advance in technology has made it more economical for the shipping all around the world and making it true resource for the world.

Transforming gas from its natural state into liquefied natural gas (LNG), it can be delivered via tanker or by several other sources from distant production areas to markets that need it. Because of its flexibility, environmental benefits and large resource base, LNG is a good and natural choice to help to meet the world's growing energy needs. LNG is transported at a constant temperature and pressure by several dedicated carriers, designed and built to meet the most rigorous safety standards.

Since 1959 Liquefied natural gas (LNG) is transported by sea in specially designed LNG carriers. These special vessels have shown a remarkable safety past or record and provided an important link in the movement of LNG from location of production to consumer location.

For LNG which is transported by trucks and other land vehicles, it is usually stored in specially designed cryogenic vessels. As LNG is a combustible liquid, the truck is equipped with many safety facilities as an emergency shutdown switch, fireproofing equipment, a quick melting plug, a nitrogen flashing- and filling system, a fire hydrant and grounding equipment.

Especially designed LNG ships with a double hull are used to provide optimum protection for the integrity of the cargo in the case of grounding or colloison. The ship which is carrying LNG, has safety equipment for ship handling and cargo system handling. The ship handling safety equipments help crew to monitor ship's position, traffic and are able to identify hazards in the vicinity of ship with radar and positioning system. LNG carrying ships also contain nitrogen purging, gas- and fire-detection systems, double containment tanks or leak pans and double hulled ship. (Lin et al., 2010)

Natural gas is majorly transported in the form of LNG to markets, where re-gasification occurs and is then distributed via pipeline of gas.

A pipe-in-pipe system, Invar, an alloy of iron (64 %) and nickel (36 %) known for its extremely low expansion coefficient, is the ideal material for the inner pipe, which is in contact with the liquefied gas (160 ^{0}C). This material is already widely used to manufacture the membrane containment system for one of the main families of LNG carriers. For large diameter

pipes, from 0.508 m to 1.06 m in diameter, the pipes are produced from sheets of metal which are folded into a tube shape, with the ends welded together to form a pipe section. Small diameter pipe, on the other hand, can be produced seamlessly. A fiber optic sensor housed in the annular space between the inner pipe (in contact with the LNG at -160 ^{0}C) and the outer pipe (in contact with the seawater) will ensure the necessary monitoring of the cryogenic pipeline.

The pressure of gas in pipeline typically ranges from about 13.6 barg to 101 barg depending on the type of area in which the pipeline is operating. For the safety purpose pipelines are designed to withstand very high pressure. If pipelines are located in populated areas then it operates at less than half of their design pressure level.

Gas moves through the pipeline up-to (0.44 m/s), so it takes several days to arrive at a utility receipt point. Along the way, there are several interconnections with other pipelines and other utility systems, that offer operators of system a great flexibility to moving gas. When gas in a transmission pipeline reaches a local gas utility, it normally passes through a "gate station." Three purposes are served at Gate station. Firstly, the pressure is reduced in the line from transmission pressure levels (13.6 barg - 101 barg) to distribution levels, which ranges from 0.017 barg to 10.1 barg. For detection of any leakage, an odorant (methyl mercaptan) is generally added to the gas.

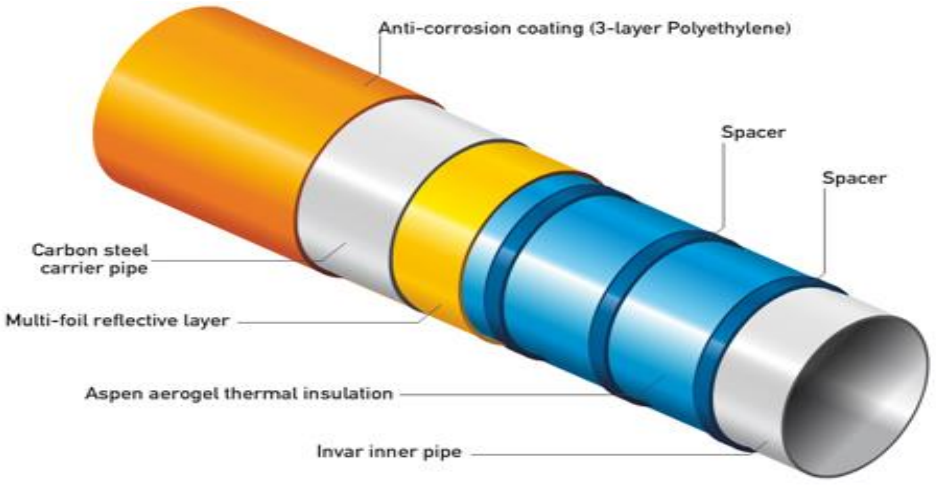

Fig.1.2. Subsea cryogenic pipeline (www.total.com)

1.3.2 Hydrate formation

In deep water i.e greater than 400 m water head, leads of hydrate the gas is formed. Gas hydrates are solid like structure in which molecule occupy almost spherical shaped holes in ice like lattice made up of hydrogen bonding between water molecules and gas molecules. The phase equilibrium diagram representing the conditions under which these gas hydrates can exist is given in Fig. 1.3. If the local temperature and pressure condition are below the equilibrium line of their phase diagram, hydrate formation occurs.

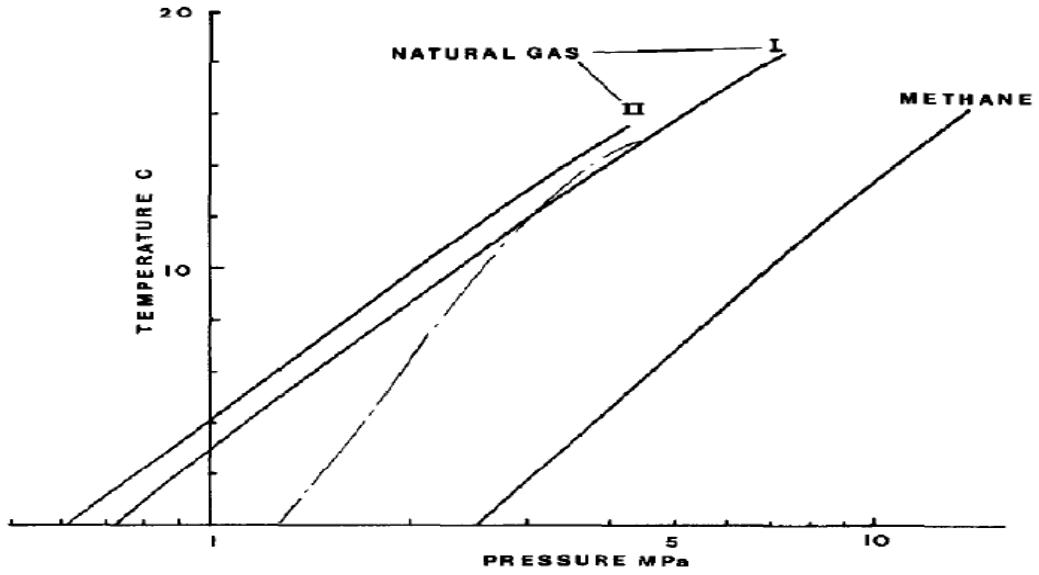

Fig.1.3 Phase equilibrium diagram for hydrocarbon gases (Topham, 1984).

The NG hydrate has "cage" like structure with a density of about 720 kg/m^3 (80% of normal ice) The methane hydrate has a density of about 840 kg/m^3. The latent heat of release is the limiting factor for hydrate formation. The latent heat of hydrate formation (440 kJ/kg hydrate) is about 30% more than the latent heat of release when ice is formed by freezing water (Topham,1983).
Hydrate formation can also occur in a pipe, which can be prevented by adding some inhibitors to pipe joints. During gas movement, the inhibitor comes in contact with the gas and prevents, the hydrate formation. Monoethylene glycol or salts in drilling fluids, are injected to compete with hydrate structure for water molecules 10 wt% of methanol should also be added.

1.3.3 Health and Safety

Low temperature associated with LNG results in a variety of effects on exposed parts of the body. If a person is not suitably protected against low temperature, the reaction and capabilities of the person can be adversely affected. Contact with LNG can produce blistering effect on skin like burning. The gas issuing from LNG is extremely cold and can cause burning. Delicate tissues like that of eyes can be severely damaged when it come in contact with this cold gas even though it would be too brief to affect the skin of hands and face. Unprotected part of a body should not touch the un-insulated pipe or vessel containing LNG. Prolonged breathing in extremely cold atmosphere can cause damage to lungs and short exposure can cause breathing discomfort.

This gas is asphyxiant, and, therefore, so the higher concentration of gas results in nausea and dizziness due to anoxia. The fire extinguishers of dry powder type are conveniently available when handling LNG (CEE, 2003).

1.4 Leakage of LNG

LNG cannot burn in its liquid state and is not an explosive too. LNG vapors which consists of mainly methane (natural gas), can only burn in the narrow range of a 5% (LFL) to 15% (UFL) gas-to-air mixture. LNG will not burn if the concentration of fuel is below 5% due to insufficient fuel and if concentration is greater than 15%. LNG when exposed to ignition source burns if it mixes with air in the flammable ratio in the above percentage range. When LNG is released in the atmosphere, it appears as a white cloud, the LNG vapors will warm and become lighter than air, and disperse with the prevailing wind. The cold LNG vapors will appear as a white cloud. If on spilling the LNG vapor does not ignite, it would result in concentration build up. As the concentration increases asphyxiation hazard of methane exposure will result.

If spilling or leaking is followed by a vaporization event in a marine environment, then an explosion may occur if methane concentration will reach to its peak proximity along with a source of ignition. LNG pool can vaporizes faster than an equal sized pool on land and the LNG can undergo “rapid phase transition”, which is a physical explosion of vapors (not a combustion). On ignition, the LNG pool formation occurs. On burning, there is a cloud formation in case of Natural gas.

Gas release process is affected by depressurization mode of pipe section and by the mode and final configuration of rupture. Fluid release from high pressure pipeline is assumed to be compressible flows. The blowout of gas underwater results in a formation of jet which moves due to discharge of momentum. The jet or plume region is confined to the area of sea-bed and is relatively very short in length generally less than one meter. Because of density difference between expanding gas bubble in plume and water buoyant force is created, due to which plume moves upward. This NG plume is similar to a thermal plume, and it also contains bubbles which results in formation of two layers, radial structure with an inner core of bubble plume and an outer ring of which contains entrained water. The ambient sea water gets continuously entrained into rising plume because of velocity difference between the plume and water. Entrainment decreases the plume velocity and buoyancy with the simultaneous increase in its radius. Due to turbulence, bubbles in plume breakup into smaller bubbles and the droplet size varies from a few micrometers to millimeters, and they are rapidly transported upward by rising plume. There is no contribution of bubble rise velocity to upward motion. As this rising plume reaches the surface, it gets deflected in a radial direction, without any appreciable loss in momentum. This rising radial jet, with its origin at sea surface flow zone generally is in the vicinity of blowouts, and carries particles rapidly away from the centre of the plume. If this buoyant driving force for the plume is dissipated by entrainment before it reaches on the water surface, the liquid droplets in the plume will be carried to surface majorly by their own velocity and surface interaction zone will effectively disappear (Spaulding et al, 2000)

In order to achieve sound and safe operation of natural gas pipelines, routine inspection is done to check corrosion and defects. This inspection is done through an equipment known as ‘smart pigs’. These pigs are robotic devices that are propelled down the pipelines to see the interior of the pipe. They check pipe roughness, roundness, thickness, detect minute leaks and other defects in the interior of the pipeline.

The leakage of natural gas from pipelines needs to be detected at an early stage, because (as stated above) small leaks can grow. It is wasteful for fuel to leak into the atmosphere, and polluting. Large leaks can destabilize structures such as platforms, endangering human lives.

When methane is released it majorly results in global warming. The climate change warming, however, affects the stability of the hydrates. It is indicated that climatic changes in the past have

led to release of methane due to destabilization of the methane hydrate if release into the atmosphere would even accelerate the climate change. Methane being around 20 times more potent than carbon dioxide as a greenhouse gas would even accelerate the climate change if released into atmosphere. Therefore, it may be necessary to study the effects of temperature fluctuations on the stability of methane hydrates and the behavior of methane after it is released.

1.5 Oscillation in LNG pipe

LNG is flow through a pipe may encounter boil off condition due to heat transfer or friction losses which then leads to formation of two-phase LNG mixture. This two-phase mixture is subjected to pressure induced oscillations. This following relation is used for Pressure change and volumetric changes,

$$\frac{p+\Delta P}{p} = \frac{V_g}{V_g+\Delta V_g} \tag{1}$$

These pressure changes act as induced force in axial direction of the pipe. An oscillating system is formed due to this highly compressed gas volume and mass of liquid. The two-phase fluid is having some natural frequency which is a function of the volumetric ratio between liquid and gas, if the ratio is reached up to 0.5 then this natural frequency reaches its minimum value. As the non-linear characteristic of ideal gas, this compressible gas volume acts as asymmetric non-linear spring and generates forces in axial direction that are non-linear in nature and result in displacement of pipe (z) as a function of time t.

In case of cylindrical pipes of radius r carrying LNG, oscillating system can be modeled in the case of free vibrations by the following second order differential equation

$$r(1-r)\rho\frac{d^2y(t)}{dt^2} + p\frac{y(t)}{1+y(t)} = 0 \tag{2}$$

On analyzing pressure waves in mixture of two-phase fluid, the difference in the amplitude of expansion and compression wave frequencies are measured. For a particular frequency, for expansion and compression amplitude are related by Lamberts function, and response is typical non-linear characteristic, which has more than one stable solution, amplitude jumping and phase switching phenomenon. If the frequency is found to be above natural frequency then resulting amplitude is negative, which means that system will oscillate one hundred and eighty degree out of phase with excitation. As the two phase LNG pipe has complicated non-linear nature, this may

result in LNG pipe oscillations and vibrations of two phase flows which are needed to be closely monitored and observed in order to maintain plant safety and to make reliable plant operation. In order to avoid oscillations the existing frequency should be kept above the natural frequency, i.e. the gas volume ratio should be kept greater than one. (Kimmel, 2006)

1.6 Subsea Plume Modeling

To study about the consequences of sub-sea gas rupture and to make risk strategies, it is very necessary to understand the quantitative impact of the released gas. As realistic experiments are quite expensive and potentially very dangerous, quantitative models have been developed as interesting tools for research. The aim of modeling sub-sea dispersion is to provide properties such as width of the plume and the mean velocities at the sea surface in order to provide input to models which are capable of quantifying hazards.

Three methods or models, of different complexity, have been used in modeling the discharge of release from sub-sea gas pipe. These of discharge models are:

- Empirical/ Cone model
- Integral Model
- Computational Fluid Dynamic (CFD) model

1.6.1 Empirical/Cone Models

Empirical models are considered to be the simplest form of modeling which can be applied to subsea releases, these models assume that the bubble plume which is dispersing can be shown or represented as a cone of fixed angle. The cone model assumes that the plume of bubble which is rising will occupy a cone of angle θ, or, at surface radius is equivalently in a fixed proportion of depth. A relation like: $b(z) = z \tan(\theta/2)$ is generally used which is shown in figure 1.4.

The angle θ , and hence tan θ /2, are considered to be fixed parameters which are independent of depth and the rate of release. The value of this constant varies significantly. Several cone angles are used, typically in the range of 10 - 12^0. An angle of 10^0 is given by Wilson (1988) and Milgram and Erb (1984). For sub-sea plume, this cone angle is described and this does not include radial flow effects. The

cone model does not consider the effect of release rate on cone angle and thus for a given release depth, the diameter of the plume at the surface will be the same for pin-hole leak from

risers. These models provide solution for estimation of radius and gas velocity for sub-sea release.

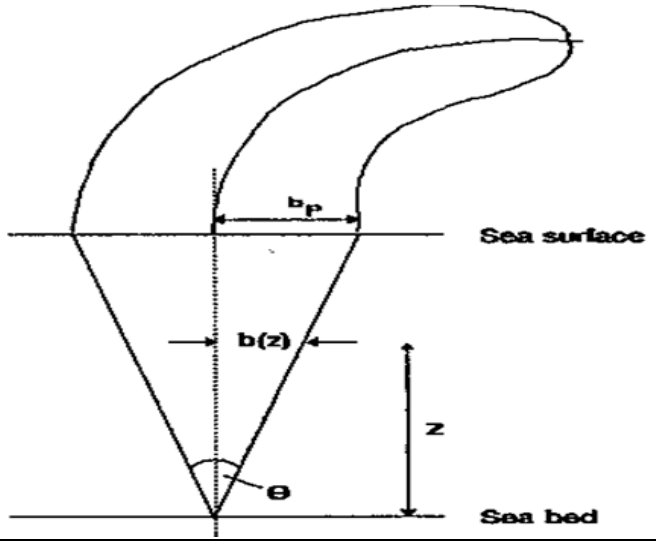

Fig 1.4 Subsea discharge based on simple cone model (Rew et al., 1995; Sridher, 2011)

NOTE:

b_p is radius of subsea plume at surface,

$b(z)$ is radius of subsea plume as a function of depth, and

z is the depth.

These models are clearly the simplest of those considered, and have the following limitations:

- They assumed complete plume similarity through depth of sea and mass flow rate of release;
- The diameter of the surfacing plume is independent of the release rate;
- No measurements were provided for the velocity and concentration of the released gas as the release occur on the surface;
- Some uncertainty also exists in the effective diameter at the surface, a factor of two is recommended.

In view of these limitations, accuracy of the results was always doubtful.

1.6.2 Integral Method

A good representation is done for bubble plume which is rising from sea is by accurate tuning of coefficient by integral methods. The major limitation of this model is that it does not give any result for surface behaviour, because at surface, only plume interacts with the floating installation, ships and offshore structures.

Physical processes are used to develop the integral models. It is assumed that the bubbles and plume dynamics are similar in manner that are used for buoyant plumes which are thermally supported.

The transient behavior leads to the generation of a large spherical cap on top of rising plume initially. It is assumed that the starting bubble plume can be characterized as large spherical bubble 'cloud' with high gas fraction, rising towards the free surface, followed by conical region. The dispersion of the gas from the release point to the surface is considered in three zones as shown in fig. 1.5(Rew et al., 1995; Sridher, 2011)

Zone of Flow Establishment (ZOFE): This region is defined between the leakage point and height from where dispersion appears to begin with a structure which resembles like a plume. This is the height at which effects are considered to be secondary for initial release of momentum as compared to momentum which is induced due to buoyancy.

Zone of Established Flow (ZOEF): This plume-like dispersion region which starts from the ZOFE from a depth below the water surface which has the same magnitude as of order of diameter of plume.

Zone of Surface Flow (ZOSF): This is the region above the ZOEF where the plume interacts with the water surface which resulted in causing the widening of the plume of gas and there is flow of water on surface radially.

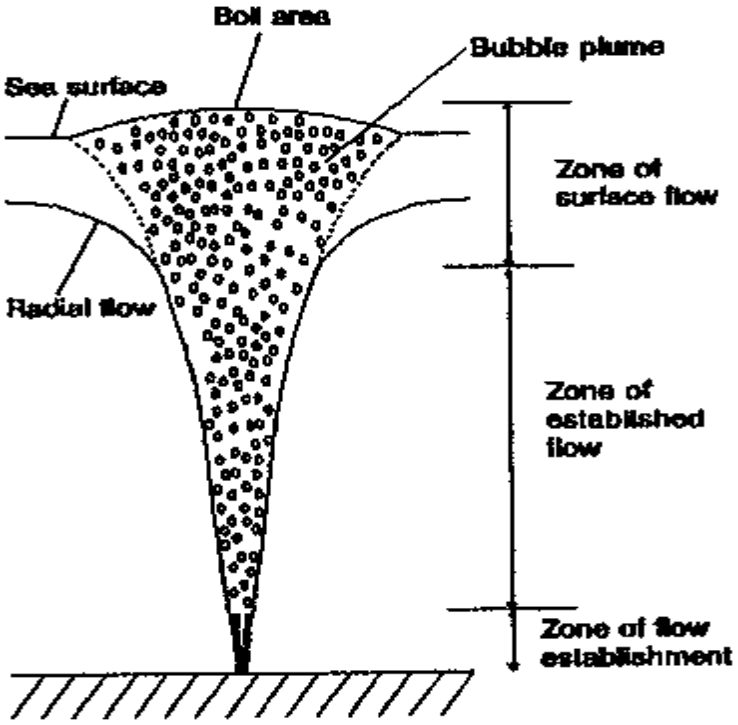

Fig. 1.5: Diagram showing different zones of sub-sea bubble plume (Rew et al., 1995; Sridher, 2011).

The radial profiles for density and velocity were assumed to have the same form at varying heights within the structure of the plume. The plume properties are represented, by using Gaussian profiles for example, centre-line properties for plume. Unsteady equations for momentum and mass conservation for rising spherical bubbles are developed and coupled to similar equations of conservation for plume. The interface region between these two is defined as a circular disk, with a net flux of gas from plume into spherical capped shape structure.

There is a correlation which relates the rate of increase of the plume centre-line properties and water flow by the use of an entrainment coefficient, which can be used for including the entrainment of water (liquid entrainment) in modeling the single phase plume. Equations for gas continuity, on relating with the equation for momentum results in the increase of the buoyancy forces, allows the plume properties to be estimated in step-wise manner as the height of release is continually increasing (Fannelop et al., 1980).

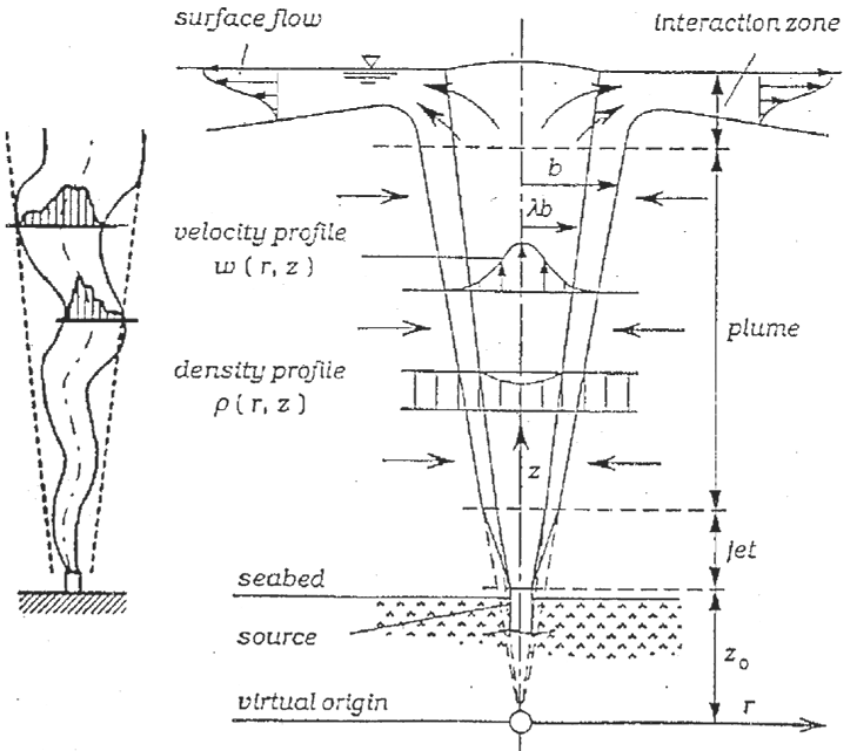

Fig.1.6. Steady-state bubble plumes with surface flow. Left: instantaneous sketch; Right: time-averaged representation, (Fannelop et al., 2007).

Fig 1.6 shows the steady state bubble plume with surface flow. Here the symbol 'z' is used to denote the distance from the source and the symbol 'r' is used for denoting the horizontal distance from the axis of the plume. An over bar is used to represent all quantities which are functions of both r and z, while this over bar is omitted for quantities which are dependent only on z. The subscript (o) is used for source values. The subscript (p) is used for representing plume quantities, while the water and gas phases are subscripted with the indices (w) and (g) respectively.

The polytropic relation is used for representing gas expansion:

$$\frac{\rho_g(z)}{\rho_g(o)} = \left[\frac{P(z)}{P(o)}\right]^{1/n} \tag{3}$$

Momentum equation for plume is given as (Fannelop et al., 2007)

$$\frac{d(\Phi_2 w^2 b^2)}{dz} = \frac{\Phi_4 g V_o}{\Pi(w+\Phi_4 w_s)}\left[\frac{H}{H-z}\right]^{1/n} \tag{4}$$

The entrainment coefficient α is observed to increase with increasing rate for gas flow. This can be shown by the means of a semi-empirical correlation which was proposed by Milgram,(1983)

$$\alpha = K\frac{F_r}{A+F_r} \tag{5}$$

Variation of range of width ratio λ which is smaller and its effect on the development of plume is of less importance. The lower value of entrainment coefficient corresponds to laboratory experiments, whereas λ is expected to approach unity for large scales.

The ratio of total momentum flux to the momentum flux is known as momentum amplification factor which is carried by the mean flow which is used to measure flux due to momentum which is dependent on turbulent fluctuations. In case of small scale experiment these parameters posses' large values and this is also described as plume wandering. On comparing the plume dimension with dynamics of bubble and have interactions which are less important, so flow starts behaving like single-phase fluid. This shows that Momentum amplification factor value will reach up to unity. Milgram,(1983).

Integral model for ZOEF:

Gaussian distribution was assumed for mean fluid velocity and the mean density defect which are considered within the plume are shown below, i.e.

$$U(r,z) = U(z)e^{r^2/b^2} \tag{6}$$

$$\rho_w - \rho_p(r,z) = S(z)e\lambda^{2r^2/b^2} \tag{7}$$

Rew et al.(l995) have solved equations using simple finite difference numerical integration scheme which is used for approximating z derivatives and then solved for the centre line velocity U(z) centre line gas fraction S(z), and the plume width b(z) using Newton iteration.

$$2\alpha U(z)b(z) = \frac{d}{dz}\left[U(z)b^2(z) - \left\{\frac{\lambda^2 S(z)}{(1+\lambda^2)(\rho_w+\rho_g(z)}\right\}\right] \tag{8}$$

$$\frac{q_T H_T}{H_B - 2} = \frac{\Pi\lambda^2 b^2(z)S(z)}{\rho_w - \rho_g(z)}\left[\frac{U(z)}{1+\lambda^2} + U_b\right] \tag{9}$$

Integral model for ZOSF:

For integral model the mass flux integral equation for the Zone of Surface Flow is written as:

$$m_f = \rho_w 2\Pi r \int_0^\infty V(r,z)dZ \quad (10)$$

and the momentum flux equation of the fluid is written as:

$$M_P = \rho_w 2\Pi r \int_0^\infty V^2(r,z)dZ \quad (11)$$

The limitations of Integral model are as follows:

- They need an established zone for plume like behavior.
- The assumption of entrainment coefficient and its constancy for free surface region and plume.
- The bubble plume is treated as a continuum with an assumption about dynamics of bubble.
- From experimental observation the ratio of inner gas plume radius to total plume radius (λ) was obtained.

1.6.3 Computational Fluid Dynamic (CFD) Model

A CFD code consists of three elements, namely the pre-processor, solver and post-processor. A geometry created in the preprocessor is read into the solver (FLUENT) where required models are selected and tuned to fit the problem. A set of equation is solved to yield a converged set of discrete solution of problem. The discrete solution must now be presented in a conceivable manner by means of post processor. This post processor provides the user interface for the solution of problem. In FLUENT, the Eulerian approach is best represented by Volume of Fluid (VOF), method. This is one of the several Eulerian models available and is especially formulated to accurately track any interface between two or more immiscible phases. FLUENT presents the Lagrangian approach as the Discrete Phase Model (DPM) and it utilizes point force Lagrangian approach. In this a stream of particle is injected into the continuous phase and then tracks them.

The CFD models used are able to find radial surface flow, which are compared well with ring vortex structure and experimental data. Multiphase computational fluid dynamic model provides a greater information on both the deforming free surface and about the bubble plume rising from

hole. Thus it is considered that these models are also very useful for predicting concentration of released gas in water (Cloete et al., 2009).

Eulerian method can be further subdivided in to mixed fluid and separated fluid formulations. In mixed fluid approach it is assumed that dispersed phase and continuous phase to be in thermal and kinetic equilibrium. It allows the use of single set of momentum equation for the entire mixture making it numerically simpler and easily applicable over a wide range of multiphase problems. VOF model also shares a single set of governing equation between phases but treatment of the interface is distinctly different from that of mixture model. The emphasis of VOF model falls on tracking the interface between phases exactly. This feature makes it ideal choice for tracking gas interface (Cloete et al., 2008).

The primary focus of VOF model is on positioning the surface between two immiscible fluids. In the domain phases are tracked through Volume fractions of the phase and in cells there is creation of continuous interface which is containing more than one phase. Two phase plume region represents a complex turbulence modeling situation. VOF Model solves for equation of conservation of mass as represented below:

$$\frac{d}{dr}(r_\Phi \rho_\Phi) + \nabla.(r_\Phi \rho_\Phi U_\Phi) = m \tag{12}$$

$$\frac{d}{dt}(r_\Phi \rho_\Phi U_\Phi) + \nabla.((r_\Phi \rho_\Phi u_\Phi U_0 - r_\Phi T_{F\Phi} \nabla. U_\Phi) = r_\Phi S_{F\Phi} \tag{13}$$

Discrete Phase Model tracks discrete particles in the whole domain by implementing force balance on every particle in lagrangian sense.

$$\frac{d\vec{U}}{dt} = F_D\left(\underset{U}{\rightarrow} - \underset{U\ P}{\rightarrow}\right) + \frac{\vec{g}(\rho_p - \rho)}{\rho_p} + \underset{F_p}{\rightarrow} \tag{14}$$

Lagrangian equation of motion for each discrete bubble was given as:

$$\rho_g(z)\frac{dV_i}{dt} = -\frac{3\mu_i}{4d_b}(V_i - U_i)C_D R_e + \rho_w U_i \frac{\partial U_i}{\partial x_i} - \frac{\rho_w}{2}\left(\frac{dV_i}{dt} - U_i \frac{\partial U_i}{\partial x_i}\right) - (\rho_w - \rho_g(z))g_i \tag{15}$$

This equation represents the balance between bubble acceleration, bubble drag, pressure gradient, bubble added inertia force and buoyancy.

Turbulence generation is modelled by assuming that production and dissipation are in balance, and that therefore total turbulent kinetic energy is generated within each cell is shown below:

$$P_b = \frac{q(z)}{N\Delta V}\sum_{n=1}^{N} F_i(V_i - U_i)dt \tag{16}$$

$$E_0 = \frac{g(\rho_l - \rho_g){d_b}^2}{\sigma} \quad (17)$$

$$C_D = \frac{2}{3}{E_o}^2 \quad (18)$$

Thus the turbulence production is due entirely to the sum over all bubbles in a cell of the power (Fi(Vi – Ui)) required to overcome bubble drag, integrated over the time taken by the bubble to traverse the cell (Sridher, 2011).

The limitations of CFD models are:

- The implementation of additional source terms in conventional CFD codes;
- The need for very specific and detailed flow data for validation purposes.

1.7 Problem statement

CFD model is used to study plume formed because of LNG released from a submerged gas pipe of diameter 1.06 m, pressure inside the pipe is 6890 kPa at which LNG flows with a velocity of 0.44 m/s.

1.8 Aims and Objectives

- To study various models to predict the dispersion of subsea hydrocarbon release (initial rise of plume from the sea surface and subsequent atmospheric dispersion).
- To identify the main features and limitations of the identified models.
- To provide an indication of the accuracy of each model and the appropriateness of its application.
- Modeling of bubble plume formed due to rupture of submerged gas pipe of LNG (low molecular weight) using FLUENT. To study the system of turbulence plume which potentially carries enough momentum to influence the shape of the free surface.
- To predict the effect of water current and temperature on the plume.
- To predict the concentration of gas released in water.

To study Characteristics between gas-flow rate versus radius, ocean depth versus centre line velocity, velocity Vs time using the results generated by simulation.

Chapter-2

Literature Review

Kobus, (1968) performed an experiment in a laboratory basin having a width of 8m and depth of 4.7m, on round bubble plume. For each airflow rate, profile of velocity versus radius were taken and were fitted with Gaussian curve whose width and centerline velocity were chosen so as to minimize the error between the curve and measured data. As fluctuations were there because of local turbulence and lateral wandering of plume he averaged his data over a time period of 5-minutes. As the diameter of air nozzle was small, the flow in nozzle was subsonic for airflow rate upto 0.0009 normal m^3/s. But for higher flow rates supercritical flow out of nozzle could have expanded rapidly and results in addition of momentum flux to the plume. Subsonic-orifice Gaussian-fit centerline velocity results were given for airflow rates of 0.0004 to 0.00057 normal m^3/s. width .As uncertainty associated with data so these data were used for comparison purpose with other data.

An experiment was performed with air bubble plumes in Saaninch Inlet off Vancouver Island using air-nozzle depth up to 60m and airflow rate upto 0.66 normal m^3/s. by Topham, (1975) Flow rate versus radius were measured at several heights from horizontally suspended 12m long beam on which 20 vertical current beams were supported. He averaged the data on the interval of 6 min for each current meter. The results for plume radii and centerline velocity vs. height show too many from smooth functions.

Study about the behavior of buoyant plume driven by the source of bubble. In a perspex tank which has cross-sectional area of 0.6 x 0.6 m and is filled with stratified salt solution up to height of 1.3m they carried out their experiment. At the floor of the tank a nozzle was placed wich was used for introducing air in tank. A large scale plume is simulated with making smaller size of bubble. Through this stratified environment when this plume of bubble rises then it also carries fluid which is transported vertically for smaller distance and this plume lefts some amount of fluid in horizontal direction at its own level of density. To study the effect of gas expansion and slip velocity of bubbles which are in plume and that is rising through stratified environment a plume was considered as single entity to make its first study of effect. The experiments that was

done by McDougall, (1978) revealed a complicated structure of plume in which they assumed that central part of plume is comprised of bubbles, and spreading in environment is due to outer portion of plume.

Fannelop and Sjoen, (1980) conducted an experiment in the laboratory basin having a width of 10.5 m and depth 10 m and airflow rate up to 0.022 normal m^3/s. They averaged their data over an interval of 10 minutes and measured velocity at different points. The Gaussian curve and data measured were fitted to velocity vs. radius profiles. The standard deviation of five percent was observed. Details of two different methods for obtaining Gaussian curve approximations and their results for these data are described by Sjoen (1982). The standard deviation between results of two methods is of order of 4%. They also determined both approximate similarity solutions and numerically integrated solutions to a set of equations that neglect the slip velocity of gas. They applied their theory to the conditions of their experiments to obtain a comparison between theory and experiment, and to make estimates of entrainment coefficient α. This was done by choosing a value of α that was constant, independent of depth, for each air flow rate such that the error between theory and experiment for plume radius vs. height was minimized. They used a value of 0.6 for the gas/ velocity radius ratio λ, where this was based on qualitative photographic observation of radius of gas containing region. The values of α obtained in this way increased with increased gas flow rate; being 0.075 for a gas flow rate of 0.0059 normal m^3/s and increasing gas flow rate of 0.022 normal m^3/s. the comparison between theory and experiment for centerline velocity showed that the theoretical valued averaged 15% greater than the experimental measurements.

When a gas is released buoyantly from the bottom of interior in liquid a bubble plume was formed. The geometry was considered an axisymmetric then it was observed that plume has round shaped mean cross-section. As the plume rises most part of this vertical plume is found in the region which is independent of release of gas or the upper water surface. This region is known as the Zone Of Established flow (ZOEF) and the most comprehensive theories and experimental measurements for this zone have been presented by Milgram and Burgess, (1980). The horizontal flow occurs below the surface near the vicinity which is also influenced by free surface, and this happened when plume was found to exists below the water surface. They

developed the two theory for surface flow. One theory was found to be suited at small plume radius and other at large radii. They conducted the experiment and compared between theories and experiment.

Milgram, (1983) reviewed several papers and identified reliable data. New experiments at larger scales were described and results were reported. These experimental results were combined with several reliable previous studies in order to form a data set for a range of heights from 3.66 to 50m and gas flow rates range from 0.0002 to 0.59m^3/sec. The integral theory of bubble plumes is combined with these obtained data to determine local properties of plume, fraction of momentum flux and entrainment coffecient which is carried by turbulence in velocity fluctuation. The relationship developed along with the integral theory provided a set of equation that are suitable for numerical solution of mean flow properties of bubble plume which is considered round in shape in his work. The qualitative understanding of parameters like momentum flux, entrainment coefficient and local properties of plume which are effected by turbulence so the relationship were made among them for proper understanding of plume and its influence. The integral mean-flow plume equations using Gaussian radial profiles are applicable to bubble plumes over a wide range of scales. There were four parameters in his theory u_b, α, λ, γ. Two of them, the bubble slip speed u_b and the gas/velocity radius ratio λ, can be estimated from known information and approximated to be 0.35m/s and 0.8 respectively. Semi-empirical functional relationships was made between local properties of plume and the entrainment coefficient α and for the momentum amplification factor γ have been determined. The entrainment coefficient was found to increase with increase values of gas fraction and with increasing values of characteristics length formed by 4/5 power of plume radius and the 1/5 power of mean vertical bubble speed, and to decrease with increasing values of distance between bubbles. The combination of these effect suggests that entrainment coefficient is increased is increased by the mixing action of the bubbles, which increases the ratio of the r.m.s. turbulent velocity at the entrainment interface to the mean centreline velocity. The momentum-amplification factor, which is a measure of the portion of the mean momentum flux carried by the turbulence, was found to decrease with increasing values of the characteristic vertical distance over which buoyancy causes a significant change in the momentum flux, and to increase with increasing values of the distance between bubbles.

Two phase flow which is associated with submerged pipe of gas rupture was considered. A new series of experiments was presented where laboratory experiments were done to measure the concentration of gas in bubbles rising, radial velocity of plume near water surface and liquid phase axial velocity. The results obtained were compared with Gaussian formulation which already exists, and with new numerical approximation which is based on simplified form of κ-ε turbulence model. Regarding scale dependence on laboratory generated plume some concerns were there and they presented that turbulence of bubble plume would not be consistent with single phase solution. When there is large velocity for radial flow on surface of water that leads to formation of large recirculation of continuous phase and also results in vortex ring formation. Model did not provide a detailed description of variation of depth in near surfaces and radial flows. This study which was done by Sworn and Moros, (1993) showed a simple numerical approximation theory which may provide an alternative data for underwater blowout.

A model was described for bubble plume rising or originating from instantaneously started source of gas at sea bed. Values for empirical model parameters were proposed and discussed by Bettelini and Fannelop, (1993). In their model starting plume was considered as growing stage at steady state then plume preceded by a spherical cap of diameter 60 m. with velocity of 4.7 m/sec and void fraction of 4.4%, which roughly behaves roughly like thermal. The sudden release was having a flow rate of 100 kg/sec. at a depth of 150 m. Integration was used to solve the governing equations numerically and the results were compared with similar solutions that were available and with available experimental data. The model performed satisfactorily, but for improving empirical inputs further experimental investigations were required. The results obtained showed that at sudden release of gas from the sea bed would affect large area.

The study about the derivation and closing of the model equation was done and this work was performed by Manninen and Taivassalo, (1996). Continuity equation and momentum equation were written for each phase in multiple phase system. The mixture equations largely resemble those for a single-phase flow but are represented in terms of the mixture density and velocity. In mixture momentum equation there is some additional term due to slip of dispersed phase relative to continuous flow. The terms for viscous and turbulent stress in mixture momentum equation are usually combined to generalized stress. In multiphase mixture, gravity and centrifugal force

tend to cause velocity difference. A group of models have been developed on the basis of assumption of local equilibrium. Depending on exact formulation of velocity the model is known as drift-flux model, algebraic-slip model, mixture model, suspension model, diffusion model and local equilibrium model. These models are given in the form of continuity equation for each phase and momentum equation for mixture with additional term which represents the effect of difference between phases. In their report they reviewed about theory and application of mixture model in dispersed multiphase flow. Manninen and Taivassalo, (1996) also studied about modeling of multiphase in commercial computer code in that they included PHONICS, FLUENT, CFX. FLUENT contains both Eulerian and Lagrangian description of multiphase flow. Mixture modelling in Fluent has been made by Johansen et al., (1990). The models developed by him are not available in the commercial code. The scalar transport equations can be used to implement the mixture model. The mixture model can be applied in flows for wide ranges of the velocity difference, particle size and density ratios as long as the force equilibrium is achieved, i.e., particles reach the terminal velocity in a short time compared to the time scale characterising the flow. The mixture model is best suited for small particles or bubbles in liquids. Implementation of the mixture model in an existing CFD solver is good and it involves the diffusion stress term in mixture momentum equation.

Physically-based phenomelogical model of jet fires for predicting size and position of fires resulting from underground gas pipe rupture was studied by Cleaver et al., 2001 and predict thermal radiation. The application of complete model to underground pipeline ruptures have made possible by the development of crater source. They undertook international collaboration of gas companies, as part of programme of research to obtain information on consequences of accidental gas release from transmission pipelines. They studied about radiation field from the flame surface based on calculated internal structure of fire. Effect of wind speed was also studied and tilting of flame was observed.

Rensen and Roig, (2001) conducted an experiment and studied about 2-dimensional bubble plumes in a tank which is confined. The bubble plume was generated in a square tank (150x150x670 mm^3). The tap water is used to fill the tank which is kept at room temperature. The bottom of the tank contains capillary tubes which contains fourteen tubes placed at an

interval of one centimeters having four rows is used to inject air bubbles from the bottom of tank. The space is maintained between rows of about 1cm. In their study they varied the gas flow rate and water depth. Some void fractions were measured in order to check mean flow of plume whether it is two dimensional or not. There are periodic oscillations which plume suffers. Video cameras and Optical fibers are used to study non stationary behavior of plume. Both front moves in phase for large gas flow rates and plume's geometric centre moves periodically which is represented like progressive wave. Eulerian measurement was used at low rates of gas flow so to calculate mean averaged data is used. Based on experimental observation a distinction is made between "low" and "high" gas flow rate, both frontiers were considered at low gas rate. They compared their non-dimensional analysis with other experiment (Delnoij et al., (1994) and Becker et al., (1997). Delnoij and Becker studied the frequency of bubble plumes which is wandering in water with gas velocity, bubble diameters, and geometrical conditions. The results of comparison revealed that buoyancy is used to control the rising plume.

Chahed et al., (2002) presented dynamic interaction between phases by using Eulerian-Eulerian two fluid models. Due to entrainment of liquid mass is added so turbulence of mass force which is added is taken into consideration for the expression of liquid force exerting on the bubbles which shows that there is significant contribution of turbulence in interfacial transfer during phase distribution. Due to bubbly flow turbulence model was developed and continuous phase Reynold stress tensor of divided in two parts, turbulent by gradient of velocity and through wakes of bubbles and there is bubble displacement due to pseudo turbulence non dissipative and each part has its own equation of transport. The model was used for simulating of three bubbly flows (uniform shear, grid, and bubbly wake) improved the representation of interaction between phases by introducing turbulent expression. This model could make it possible that the specific scale is used to describe bubble structure effect on turbulence of liquid. The numerical results represented an adequate behavior of model in both homogenous and non-homogenous turbulence. Comparison of the numerical results with the experimental data gives a good prediction about fluctuating and mean velocities and of distribution of phase. Bubble was induced by agitation which result in enhancing intensity of turbulence and on other hand attenuation in shear stress occur due to stretching of eddy.

Gases released in deep water can lose considerable amount of gas phase due to dissolution in water. Zheng and Yapa in 2002 observed dissolution of gas which has significant impact on gas behavior because of its effect on buoyancy. Simulations were presented to show effects or impact of gas dissolution on behavior of plume. Results were studied on comparing ideal gas conditions with non-ideal gas conditions.

An experiment was conducted in a deep spill in the Norwegian Sea at (65 ^{0}00N', 04 ^{0}50 E') at Helland Hansen site where depth of water was roughly in 844 m and have 125 km off the coast of central Norway. In later days of June 2000 four controlled discharges of gas and oil were made amounting 10,000 standard m^3 of natural gas and 120 m^3 of oil. The objective of the experiment which was conducted by Johansen et al., (2003) was to calibrate models which are numerically tested for subsurface surveillance. Several observations were made on winds, water density, currents, sub-surface and surface oil concentration, and biological and chemical samples in the water column and their results showed on surface oil started to reach within an hour after the discharge began and within a range of hundred of meters from the release site. Oil continued to surface for larger time after discharged has stopped. According to thermodynamic equilibrium gas hydrate should be formed but this did not happen. As it was also seen that no gas bubble reached the surface which means that dissolution of gas occur was complete but not as fast as standard algorithm which were predicted. The research vessels on echo sounders were able to track the oil/gas as plume rises through water from release.

The CFD simulation was carried out for simulating turbulence and bubble plume in water. Enhanced κ-ε turbulence model was used for two fluid, with an extra source term introduced to account for interaction between liquid and bubble and to carry out transient calculation which have been done to study the growth of plume, approach towards steady-state condition and the acceleration of liquid due to viscous drag. Experiment was conducted and spreading of plume was observed by Dhotre et al., (2007) and it was seen that turbulent dispersion and lift forces which are interfacial forces plays an important role. Sensitivity analysis for drag coefficient and for turbulent dispersions were also seen. Commercial CFD software with code CFX-4.3 was used to solve the equation of mass and momentum. Sensitivity was observed for computational grid size and it was obtained that results were independent of grid size. Two dimensional axial symmetric rectangular grids was created along with three dimensional grid. Simulations were

carried out at different heights, by varying void fractions. It was seen that a strong recirculation surrounds the plume in liquid. Both 2D and 3D simulation showed a fast upward moving bubble plume and recirculation of liquid which is surrounding the plume, driven by entrainment of liquid within plume. The flow pattern was established in column for development is gas void fraction, liquid circulation and liquid entrainment.

A three dimensional, transient model was developed in order to simulate the plume and to study free surface behavior from rupture of submerged gas pipe. A coupled Volume of Fluid (VOF) and Discrete Phase Model (DPM) was used for multiphase approach. The turbulence was modeled using standard κ-ε approach. The model which was developed by Cloete et al., (2009) was compared to experimental results and experiment was conducted in a basin of depth 7m and surface area of 6mX9m. Water was used to fill their basin and from bottom air was released at the bottom at gas rates of 83, 170 and 750 Nl/s. The air inlet was especially made and has release valve which has piston which are rapidly acting on gas which is injected vertically to reduce the vertical momentum of gas. This model was applied to release of gas at deep ocean depths to show its verification with realistic scenarios. They include the profile of plume velocity, rise time of bubble plume and fountain height. DPM did not modeled void fraction that was occupied by bubbles because of momentum over prediction which is transferred from bubbles to liquid phase. This over prediction was observed at high flow rates of gas.

Olsen and Cloete, (2009) worked on the modeling of gas stirred ladles with the assumption of flat liquid surface. They discussed about Eulerian-Eulerian- and Lagrangian method in which the bubbles are treated as Lagrangian particles Eulerian phase considered are and the liquid and the top gas with a sharp interface. They applied a method of VOF model for the top gas and liquid with Lagrangian bubbles so they can interact and can be implemented along with DPM. This coupled DPM and VOF model can be applied to gas stirred ladles with injecting at bottom and then validated against experiments. Modeling of ladle hydrodynamics with free surface dynamic is very challenging as it requires the combination of both dispersed phases with a large scale interface as multiphase approach at the liquid surface. A combination of Eulerian and Lagrangian method was applied successfully to both subsea gas release and ladle refining. The bubble plume modeling accounts for forces like buoyancy and drag, along with lift force. It was also shown

that the flat surface assumption was acceptable if the purpose was to obtain velocity profiles at various locations in the ladle. The results showed that assumption of flat surface yielded lower mixing time than the simulation with dynamic surface at various gas rates. Due to viscous dissipation large amount of energy was found to be lost because the formation of fountain of plume that require the flow to go up and then it make a very sharp turn to go back down. When the surface is forced to be flat then the flow will simply take a right turn regardless of the strength of plume.

A computer software solution was developed by SINTEF, (2009) to model the behavior of dry or wet gas from a single-phase sub-sea pipeline release from bottom surface sea to harmless with concentration of air. The special designed software was used to model the behavior of released gas due to rupture from sub-sea pipeline as they rises from the discharge point, throughout the water column, and then exits at free water surface and then disperses in the atmosphere. By sensitivity analysis of gas effects and its input from environment ultimate fate of gas was decided. From a small hole on pipeline which is under the sea release rate vs time of gas was plotted. They also developed and implemented the algorithms to predict the three-dimensional (3D) behavior as gas rises from bottom of sea to free surface of water so that they can predict the source strength and area of the gas on the surface throughout the life of the discharge. WCDgas_2.0 was used to model. WCDgas_2.0_Setup.exe file was run and they followed some other steps and obtained their result.

ANSYS CFX simulation was done to model LNG vapor dispersion in atmosphere by Qi et al., in 2010, and they also performed a set of medium scale LNG spill test at Brayton Fire Training field to validate their simulation. The effect of geometry features on vapor cloud were also represented. They also conducted an underwater test release of LNG in (2011) to understand the phenomenon of plume, they conducted an experiment in a pit of dimension 10.06 m x 6.4m and 1.22m depth. Data was collected as a function of time at several numbers of locations. Water surface and in-air phenomenon were captured by three video cameras which were placed on land. Poles which are located inside pit is provided with number of thermo couples. These thermocouples measures both temperature of water and above water surface. The concentration was recorded on poles by the sensors placed on poles within air and pit.

Li et al., (2012) studied about release of natural gas by using FLUENT and they studied by varying wind velocity upto 5 m/s. They studied about the risk area and compared their result with experimental verification.

The bubble plume which is typically the form of bubble flow is one of the transport phenomenon that have the capability to drive a large-scale convection due to the buoyancy of the bubbles. The technique of using a surface flow generated by the bubble plume is utilized as an effective way to control and collect surface floating substances in naval systems, lakes, seas, rivers, oceans especially the oil layer formed during large oil spill accidents. Abdulmouti and Jassim, (2013) researched about applications of bubbly flow and gas-liquid two-phase flow, the differences of surface flow generation mechanisms among single-phase liquid jet, single phase buoyant plume, and bubble plume. The flow depends on the gas flow rate, the bubble size, void fraction, bubble velocity and the internal two-phase flow structure of the bubble plume. They also carried out a laboratory experiment to investigate about multidimensional motion of water and bubbles. The experimental setup include inner tank size is 1300 mm in length, 1000 mm in height, and 110 mm wide, made of transparent acrylic resin. The data was obtained by applying image processing and Particle Imaging Velocimetry (PIV) measurements to two kinds of visualized images: The first is visualization of the whole field around the bubble plume, and the second is that of the flow structure of bubble for the different sections of bubble regions. The flow pattern for the whole field flow structure of the bubble plume is demonstrated. The flow structure is sensitively modulated by the gas flow rate and bubble size and their result shows that there are two large circulation flow regions of liquid near the bubble plume. Inside the bubble plume and near the free surface, the velocity of the two-phase flow is higher while it is slower in other regions. The generation of this high speed flow is considered a main contribution to induce a strong surface flow. The highest kinetic energy is generated at a long distance (far up) inside the bubble plume and in the vicinity of the free surface. High vorticity distribution is generated by the surface flow, which induced by the bubble plume, and these phenomena appear in a layer under the free surface.

A plume in water body a model based on random theory of medium and on model of acoustic velocity of bubble medium was studied by Ping et al., (2013), they also study the gas hydrate bubble plume seismic responses produced in cold seepage active region. The acoustic wave

velocity satisfied that the variation of velocity is related to bubble radius and contents. The bubble radius and content varies with sea depth. The plume in water body was simulated by finite difference solving two dimensional acoustic wave equation. The scattered energy of wave is strong at place where plume exists. The place where scattered wave energy is stronger, minimum time will occur for travelling the plume. Sesmic records of the shots gathers were processed by pre-stack time migration. The aim of building model is to study the seismic responses produced by plumes, model design need not only practical significance but also proper simplification about real plume. The study results in foundation for further study of seismic responses that are produced by plumes and they provided a new approach for identification of gas hydrates.

2.1 Citation report

(Published and Citations graph in each year of latest 20 years in Modeling of Bubble Plume from Web Of Science as accessed on 22 september,2013, http://apps.webofknowledge.com)

During the citation report Web of Science with the modeling of bubble plume as the keyword. The search showed 397 results with a total citation of 6464. Average citation per index is 16.28. The h index is 38. The graphs obtained are shown below:

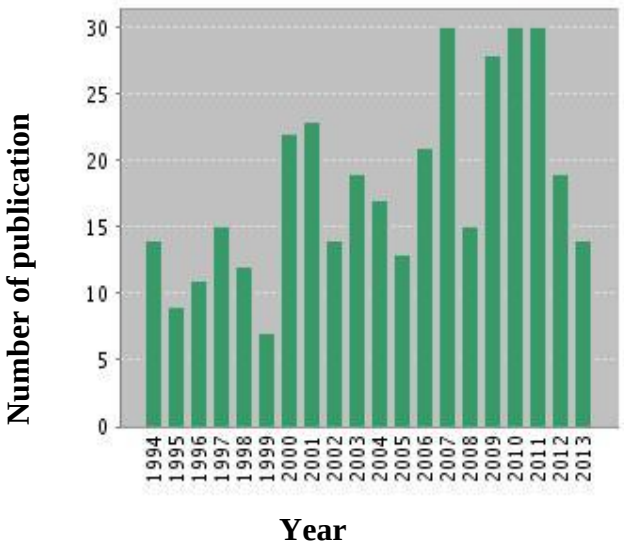

Fig. 2.1a: Published items in each year on the topic of modeling of bubble plume.

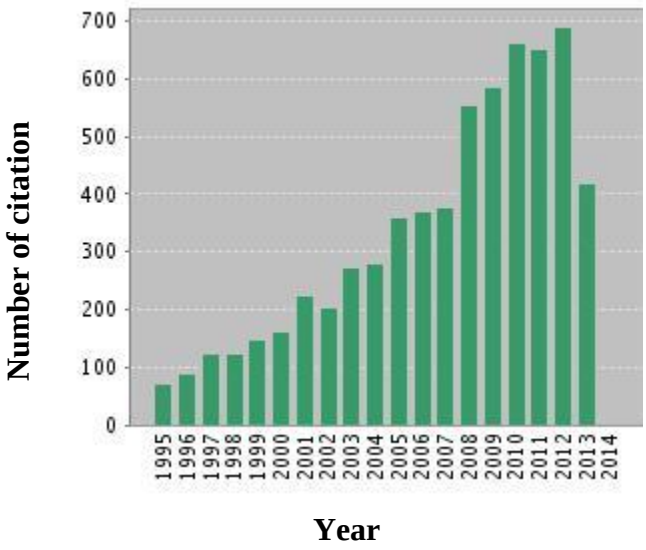

Fig 2.1 b: Citations of articles in each year on topic of modeling of bubble plume

From the above graph we can see that maximum articles were published in the year of 2007, 2010 and 2012. This includes every field where ever bubble plume can be generated. Publications are there in many journals and conference reports for bubble plumes generated in various fields.

In the Web of Science when bubble plume formed under water was used as a keyword, 12 results were obtained with a citation of 512. The average citations per item is 42.67. and the h-index is 9

.

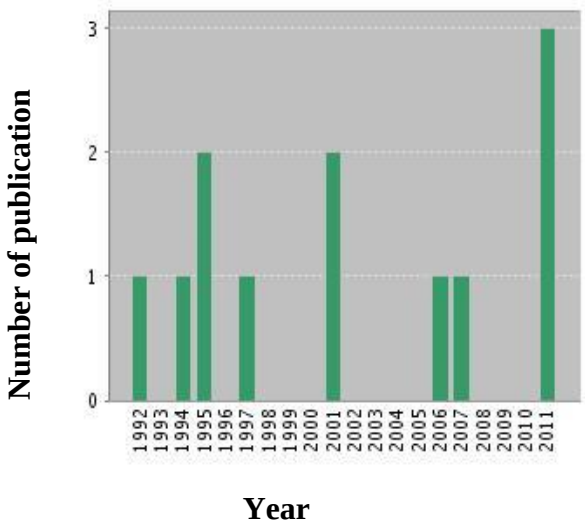

Fig 2.2 a: Published in each year on the topic bubble plume formed under water

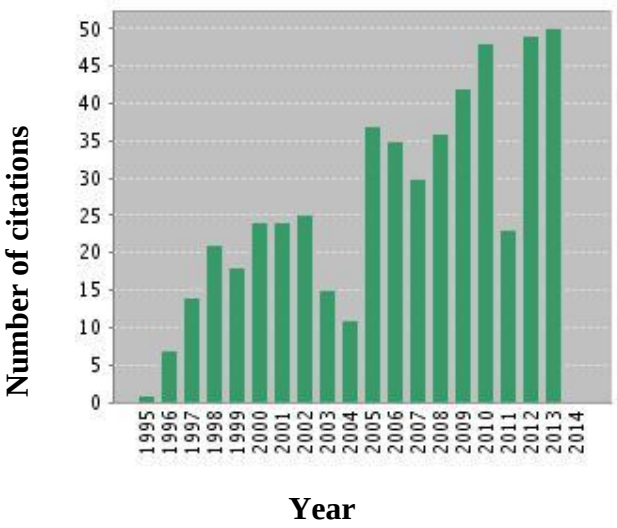

Fig 2.2 b: Citation in each year on the topic of bubble plume formed under water.

In web of science with the keyword gas pipe under water resulted in 290 publications with a citation of 2332. The average citation per item is 8.04 and the h-index is 24. This shows that the topic is under intense research. Please see figure 2.3

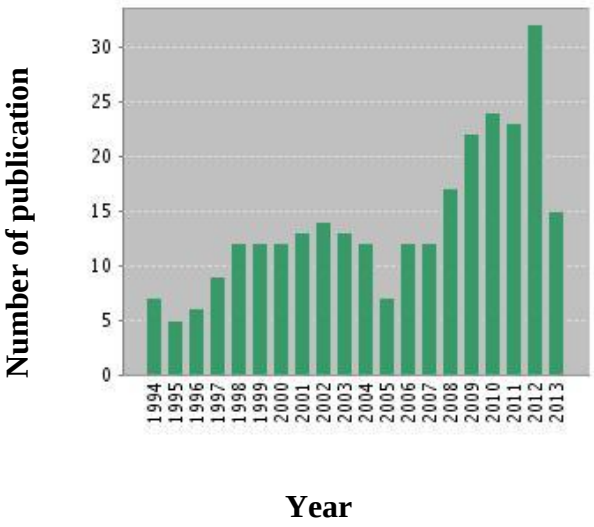

Fig 2.3 a: Published articles in each year on topic of gas pipe under water.

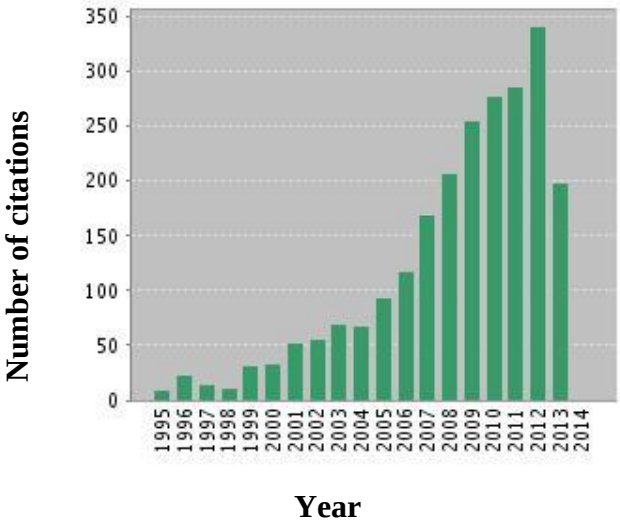

Fig 2.3 b: Citations in each year on topic of gas pipe under water.

In web science with the keyword hydrocarbon release under water, 24 papers/studies are shown with a citation of 631. The average citation per item is 26.29. The h index obtained is 12. In the citation graph we can see that articles related to the topic have been cited many times and in year 2012 citation reached to its peak. From 2008 to 2013 citation graph shows that the topic have been studied quite frequently.

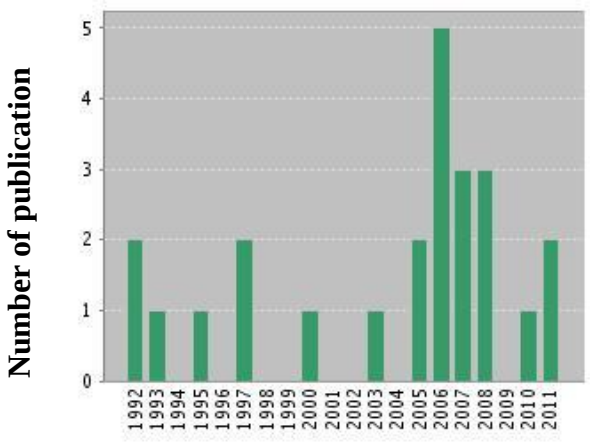

Fig 2.4 a: Publications of articles in each year on the topic hydrocarbon release under water.

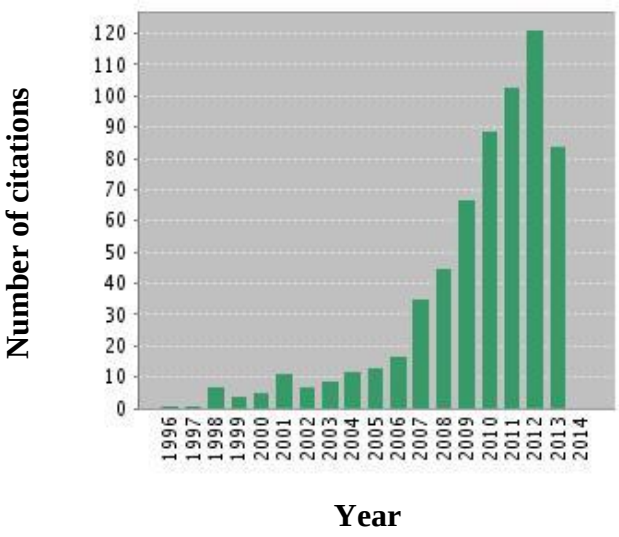

Fig 2.4 b: Citations in each year on the topic hydrocarbon release under water.

Chapter-3

Modeling and Simulation of LNG from under sea submerged pipeline

The model is designed to study the system of bubble plume which rises carrying enough momentum to influence the shape of free surface.

The regulatory agency, US Department of Transportation (DOT), has expressed concern over possible LNG leaks from pipelines in to water column and has shown that current models are not sufficient to quantify the potential hazard from leaks. As the information about release of LNG is very limited so for the study we will use the correlations that are given in the paper of Raj and Bowdoin, (2010) theoretical model.

In our study we assumed LNG transmission pipeline of 42 inch diameter having pressure of 1000 psia. The temperature of LNG is kept below the boiling temperature, but due to movement of gas in pipe there is a boil off condition due to friction losses and heat transfer.

The general equation of continuity and momentum balance under turbulent conditions are given as:

Equation of continuity:

$$\frac{\partial \rho}{\partial t} = -(\nabla . \rho v)$$

(19)

Equation of motion:

$$\frac{\partial}{\partial t}\rho v = -[\nabla . \rho v v] - \nabla p - [\nabla . \tau] + \rho g \qquad (20)$$

For pipeline flow in axial direction, x, these equations can be reduced as:

$$\frac{\partial \rho}{\partial t} + u\frac{\partial \rho}{\partial x} + \rho\frac{\partial u}{\partial x} = 0 \qquad (21)$$

The conservation of momentum is given by Navier-stoke equation,

$$\frac{\partial(a_1\rho_1 u_i u_j)}{\partial x_j} = -a_1\frac{\partial p}{\partial x_i} + \frac{\left(a_1\mu_1\left(\frac{\partial u_i}{\partial x_j}+\frac{\partial u_j}{\partial x_i}\right)\right)}{\partial x_j} + \frac{\partial(a_1\tau_{ij})}{\partial x_j} + F_i \quad (22)$$

Release from hole is compared to orifice leakage, the mass flow rate used for calculation is same as used by release of fluid from orifice. The mass flow used is calculated by the relation,

$$\dot{m} = 0.61 Y S_o\sqrt{2(p_a - p_b)\rho_a} \quad (23)$$

$$Y = 1 - \frac{0.41+0.35\beta^4}{\gamma}\left(1 - \frac{p_b}{p_a}\right) \quad (24)$$

This equation must be used when pb/pa is less than 0.53 which is critical pressure ratio.

The LNG jet outflow velocity is given by (Raj and Bowdoin, 2010)

$$u_j = \frac{V_j}{\frac{\pi}{4}\times d_j^2} \quad (25)$$

.

The vertical distance from the leakage where the jet breaks down completely is determined by (Raj and Bowdoin, 2010).

$$S_j = 10 \times d_j \quad (26)$$

Where S_j is the vertical distance where jet completely breaks down into droplets of liquid. In our model we assume that the distance (in centimeters) of breakup of the coherent liquid jet plume is very short as compared to the depth of water (several meters) above the leakage or jet release location. It is anticipated that the sizes of droplets of LNG formed due to the domination of dynamic forces of jet in water on thermal interaction between the two.

The maximum size of liquid droplets resulted from the breakup of jet due to mechanical forces is determined by following correlation,

When $Bo_j \leq \pi^2$

$$\frac{d_p}{d_j'} = 3^{1/3}\left(\frac{\rho_j}{\rho_w}\right)^{2/9}\left[\frac{1}{\beta\sqrt{2\pi We_j}} + \frac{2^{7/2}\pi^{3/2}2}{\beta We_j\sqrt{Lp_j}}\right]^{2/9} \quad (27)$$

When $Bo_j \geq \pi^2$

$$\frac{d_p}{d_j'} = 3^{1/3}\left(\frac{\rho_j}{\rho_w}\right)^{2/9}\left[\frac{1}{\beta\sqrt{2\pi Bo_j We_j}} + \frac{2^{7/2}\pi^{3/2}2}{\beta We_j\sqrt{Lp_j}}\right]^{2/9} \quad (28)$$

Where,

$$Bo_j = \frac{g(\rho_w-\rho_j)d_j'^2}{\sigma_j} \qquad Re_j = \frac{U_j d_j'}{\vartheta_j}$$

$$We_j = \frac{\rho_j U_j^2 d_j'}{\sigma_j} \qquad Lp_j = \frac{Re_j^2}{We_j}$$

If $d_j \leq \frac{\pi\sigma_j}{g(\rho_w-\rho_j)}$

$$d_j' = d_j$$

If $d_j \geq \frac{\pi\sigma_j}{g(\rho_w-\rho_j)}$

$$d_j' \leq \frac{\pi\sigma_j}{g(\rho_w-\rho_j)}$$

ρ_w is density of water, ρ_j is density of jet liquid

Surface tension of jet is σ_j, β is constant (0.3).

The calculation for the heating of liquid droplets by using the largest size is conservative because smaller droplets can heat up faster. The laminar rise terminal velocity of largest droplet is given by,

$$U_d = g\frac{1-\frac{\rho_L}{\rho_w}}{18\vartheta_w}d_p^2 \quad (29)$$

Turbulent rise velocity is given by,

$$U_d = \sqrt{\frac{4}{3}\left[\frac{g\left(1-\frac{\rho_L}{\rho_w}\right)d_p}{C_D}\right]} \quad (30)$$

As the diameter decrease linearly with time, the complete evaporation time can be determined by,

$$t_{evap} = \frac{\lambda\rho_L d_p}{2h_{FB}(T_w-T_{sat})} \quad (31)$$

The vertical distance traveled by largest liquid droplet before it completely evaporates is given by,

$$S_d = (\frac{1}{3})U_d t_{evap} \quad (32)$$

Where S_d is the vertical distance traveled by liquid droplet before it completely evaporates (Qi et., al 2011).

As this cold vapor bubbles rises upward in the water it expands in volume because of decreasing hydrostatic pressure of water that it experience and will be continuously heated to surrounding water in sea. The model discussed below is about rising of single vapor bubble and its heat exchanging with surrounding water. The vapor present in the gas bubble is assumed to be the perfect gas. The vapor bubble from inside are always assumed to be in thermodynamic equilibrium at the local conditions of pressure. That is, a quasi steady state is assumed. The initial condition of the vapor in the bubbles is represented by the saturated condition of (LNG vapor) at the total pressure corresponding to the depth at which the bubble is initially released. The effect of changes in density of vapor on the total buoyancy force of the bubble can be ignored (because the vapor density is small as compared to density of water). The vapor bubble can be represented as small sphere characteristically. That is, the size of vapor bubble is represented by an equivalent diameter of sphere, even though the bubble itself may have different shape than that of a sphere. With its "current" diameter bubbles rises with its turbulent terminal velocity in consistency. The motion of vapor within the bubble is neglected because of its effect on rise velocity. The mass of vapor in the bubble is constant during its rise through the water column. No absorption of gas is there. All the bubbles which are rising can interact with water independent of other bubbles present in the domain. That is, no consideration is given to the "swarm" behavior of rising vapor bubbles.

3.1 Geometric model

In our study we choose the diameter of pipe is 1.06 m which is undersea, the pressure inside pipe is 6890 kPa in which LNG is flowing with a velocity of 0.44 m/sec if it remains liquid. In case of boil off condition velocity rises up to 1 to 4 m/s. The temperature inside the pipe is 105 K to 115 K. Temperature outside the pipe is varying according to the depth. FLUENT's standard

preprocessor GAMBIT 2.3 is used for mesh creation. A 2 dimensional mesh is created for different hole diameter and varying depth. Hole diameter chosen for study is20 mm, 30 mm, 50 mm, 100 mm. keeping hole diameter constant depth are varied as 0.5 m, 1 m, 3 m, 4 m.

In simulation we use depth which can be scaled up in the ratio of 1:100 in real situation, that is we have depth of 50 m, 100 m, 300 m, 400 m. Meshed geometry is shown in fig.

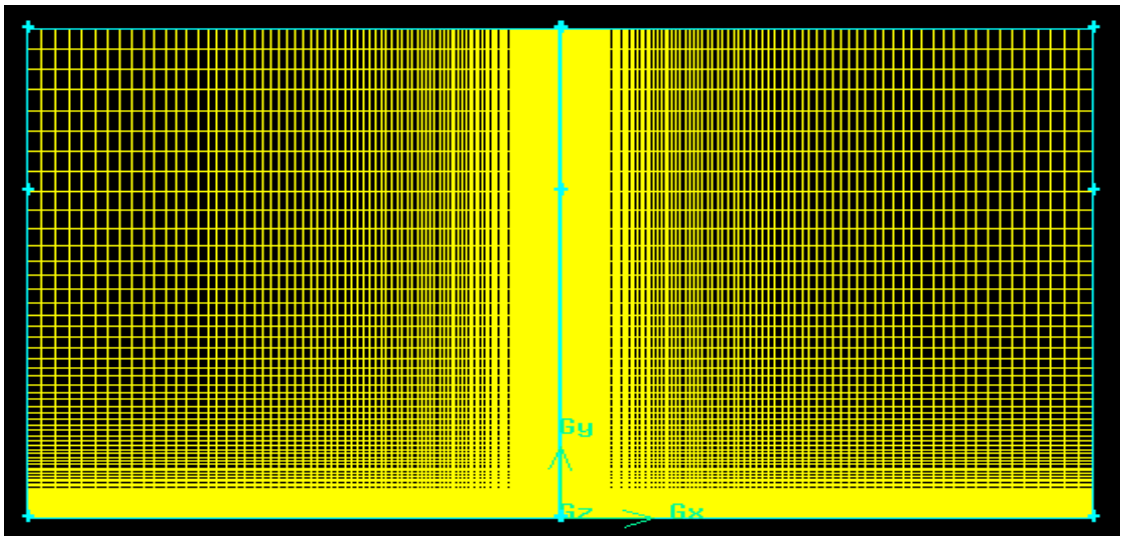

Fig.3.1. Geometric grid structure of model

The mesh shown above is of 20 mm inlet and 400 m (4m) depth. The space above is of 200 m (2 m) in which air is patched with volume fraction of 1.

The mesh has three faces, and meshing is done in geometric progression with ratios 1.025 in radial direction and 1.06 in axial direction with spacing of 0.05. This is done to have refined mesh structure near the plume area in order to capture void fraction and velocity profiles in plume region. The edge of the hole is meshed very fine with spacing of 0.005 to make our study more accurate. The above region is meshed with ratio one and 0.25 spacing. The faces are meshed with quadratic element and sub-map type.

Hole of varying sizes are given the mass-flow inlet and other edges are kept wall with no slip boundary condition. The top edges were selected as pressure outlet boundary condition. From inlet only methane is allowed to release by making other components volume fraction zero.

3.2 Solution procedure

The meshed geometry is exported to FLUENT 6.3 and read their as mesh file. After having a check on grid, we will follow the procedural steps. The multiphase model chosen is Volume of Fluid, this model adapts the continuity equation with volume fraction term, α_q, if a cell is found to consist of two or more phase, an interface must be differentiated through it. The geometric reconstruction scheme is selected as the interface interpolation method to ensure maximum accuracy in interface tracking. The implicit body force formulation was selected to improve model stability in the presence of large body forces. From FLUENT database material is chosen as per our requirement, and properties are set accordingly. Water is selected as primary phase, secondary phase is given to air and methane, and respective surface tensions are inserted in interaction panel. As surface tension is a function of density so it will vary according to depth, for different depth geometry surface tension values are inserted accordingly. If a User Defined Functions (UDF) is made for varying surface tension that can also be implemented as user defined function in interaction's surface tension panel. In boundary condition panel, the mass flow rate is set for methane by selecting inlet, and others mass flow rate is set to zero. The pressure in boundary condition panel is programmed and implemented as user defined functions. The boundary conditions table is shown:

Table 3: Values to be inserted in boundary condition panel.

Hole diameter (mm)	**Simulation-Depth (m)**	**Pressure (MPa)**	**Mass flow inlet (Kg/s)**
10	3	3	2.26
20	0.5	0.5	10
20	1	1	9.963
20	3	3	9
20	4	4	9.55
30	0.5	0.5	22.61
30	1	1	22.41
30	3	3	20.5

30	4	4	21.5
50	1	1	62.27
50	3	3	56.95
50	4	4	59.71
100	1	1	248
100	3	3	227.7
100	4	4	238.8

The top air above the water is patched with a volume fraction of one. In adapt dropdown list the region to be patched is marked, and after initialization the region is patched. In solution control panel, PISO is chosen to be pressure- velocity coupling scheme, this scheme is a part of SIMPLE family of algorithms, but completes additional iterations for skewness and neighbor correction. The faster convergence is achieved by PISO scheme and also uses significantly higher under-relaxation factor for both momentum and pressure, results in substantial reduction in number of iterations required for converging. The standard κ-ε model was implemented with default constant to model the turbulence. This model is selected because it is very easy to converge, reasonably accurate for wide range of flow rates and light on computational domain. Turbulence of the liquid phase has a very strong influence on distribution of void-fraction. Discretization of Pressure is done using PRESTO! Scheme, which is recommended for the situations having swirls and strong streamline curvatures. Discretization of continuity, turbulence and momentum equations was done using the second order upwind scheme. Convergence is judged by means of scaled residuals of flow variables, the convergence criteria is set in residuals panel of the order of 0.00001 for all the variables. Then we can allow our simulation for iterations, the time step size is set 10^{-5}, and allows thousands of iteration.

After completing all the steps for setting simulation we can make case file, and can also save our data file accordingly, which help us in looking the results again. The simulations were carried out on a grid of cells 10000 to 48000 as per hole diameter and depth, with 2GHz CPU, 64-bit windows version of FLUENT 6.3.26. For the post processing we will use FLUENT, to see the plots and contours of phases, velocity, turbulence, etc.

3.3 Assumptions

Depth is not considered more than 400 m that is 4 m simulation length, because as the depth increase pressure exerting will also increase and that may provide suitable conditions for hydrate formation, so for the simulation purpose we are avoiding depth more than 4 m.

Pure methane is assumed to be releases from the hole. The properties were used of LNG and they are inserted in the material data base in material panel for initial condition. For varying depth the properties of methane are used.

No chemical reaction or species transport is assumed. This assumption is valid since the depth is taken to be less than 400 m.

Initially for the growth of plume we assumed that there should be no energy transport. LNG vaporize quickly as it absorbs heat from the environment, and results in vapor cloud formation, that is it changes from liquid phase to gas phase instantaneously. This rapid phase change of LNG is called ‘Rapid Phase Transition (RPT)’.

For the study of plume growth, and the time it takes to reach the surface we will not use DPM for tracking of particle, once the plume is fully developed than we will inject particles to see bubble diameter.

Chapter-4

Results and Discussion

When the gas is released due to rupture we have some hazardous zones in the near-by area of release. The gas cloud released should be treated as either a free jet which is fully developed or a plume or the dispersing cloud that is affected by wind or by the atmospheric turbulence. The jet and the plume will take some time to get fully developed in the velocity and the concentration range. The measurement of concentration, velocity components, etc. can be done at numerous locations on the path of released gas in order to study the characteristic of its flow. As the jets released are colder than ambient atmosphere the Joule-Thomson effect were would result in the pressure drop in the domain of interest. The release of gas from a hole in the pipeline and the spreading of the gas in water were simulated using the commercial CFD-code. In a weakly supercritical free jet vertically issuing from a hole into domain, the contour plots of gas phase at different times during the process can be seen. The concentration of methane and how it is increasing is shown in fig. 4.1

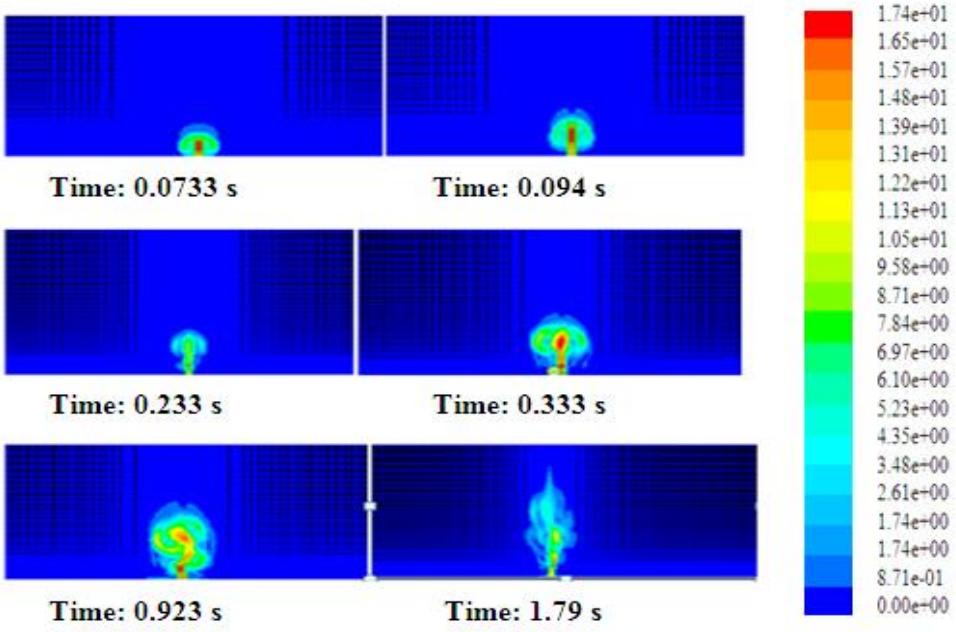

Fig.4.1 Contours of volume fraction of methane for growth of plume in the form of jet.

As we know, it is quite difficult to differentiate between a jet of liquid, droplets and vaporized droplets (vapors or gas bubble). A mushroom like cloud with long tail appears that moves very rapidly upwards to the surface of water. This rising plume is like a vertical jet of very violent plume which agitates the surrounding water. This results in high evaporation rate and a large volume of gas releases. The outlet from the hole or the leakage point contains LNG in majorly liquefied form, but turns to vapor as soon as it is released, or sometimes two phase flow may occur from leakage because vapor may also get generated within pipe due to frictional losses and heat transfer. From the figures, it is clear that as the LNG is released it gets gasified and the gas plume rises with the plume getting shattered. The plume rise is like the formation of a "mushroom" like structure near to the rupture. As this plume moves upward in the domain, it appears vey dark in color, like mushroom structure having a tail.

If the rupture occurs in a shallow depth, it may be quite possible that the jet formed due to leakage may not vaporize completely within surrounding water. Then the liquid may rise into the air like droplets of liquid along with generated vapor, resulting in formation of a fountain on the surface of water. The fountain height varies with the depth of release and the vertical length of the fountain depends on the depth and mass flow rate. After travelling some distance, the jet breaks down completely into droplets. The calculations are made for different depths (50 m, 100 m, 300 m, 400 m) and the hole diameters (20 mm, 30mm, 50 mm, 100 mm.).

4.1 Effect of varying depth on constant hole diameter

For a constant hole diameter, it is observed that the plume takes less time to reach to the surface for shallow depth, as the pressure difference between the pipe first inside the leakage hole and the environment increases resulting in increase of mass flow rate. From table 4.1 it can be observed that for a 20 mm hole diameter as the depth increases the plume width increases but decrease in fountain height. As the depth increase from 50 m depth to 100 m the fountain height decreases and the plume width increase. Similar trend was also shown for depth of 300 m and 400 m. For a small depth the fountain height is large but the plume diameter is smaller. As the depth of release increases the plume diameter also increases affecting more surface area in the process. From this we can conclude that larger the depth of release the larger free surface would be affected for the same leakage. Through the plume diameter, we can determine how much surface area is affected.

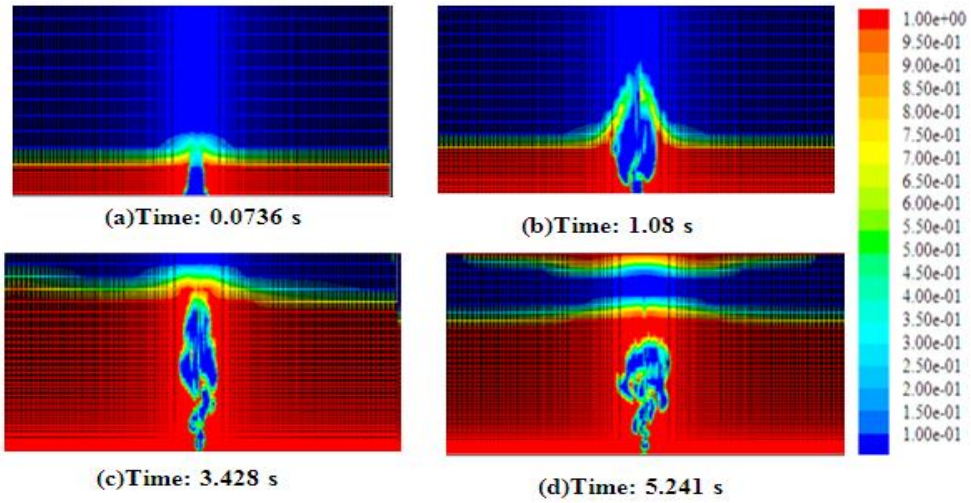

Fig.4.2: Contours of volume fraction with respect to primary phase.

Hole diameter: 20 mm; **Depth:** (a) 50 m, (b) 100 m, (c) 300 m, (d) 400 m.

The simulation results show as that the plume reaches the surface earlier for shallow depth but takes longer time as the depth increases. The intensity of darkness reflects the increasing concentration of methane.

4.2 Effect of varying hole size

In case the depth remains constant and the hole diameter is varied, it is observed that the amount of release will increase due increase in the area of release. Therefore, violent release will be observed for large rupture. Fountain height and plume width are also larger for large rupture area (or diameter). This means that the larger the rupture, larger and more pronounced gas release will take place. These observations are shown in fig. 4.3 for a leak of depth 300 m for hole diameters of 20 mm, 30 mm, 50 mm, 100 mm. The contours for 50 mm and 100 mm size holes are different than for the other two. For large hole size (area), the release forms a jet but some amount also remains also at the surface, and the releases became more violent than that for the small leakage area.

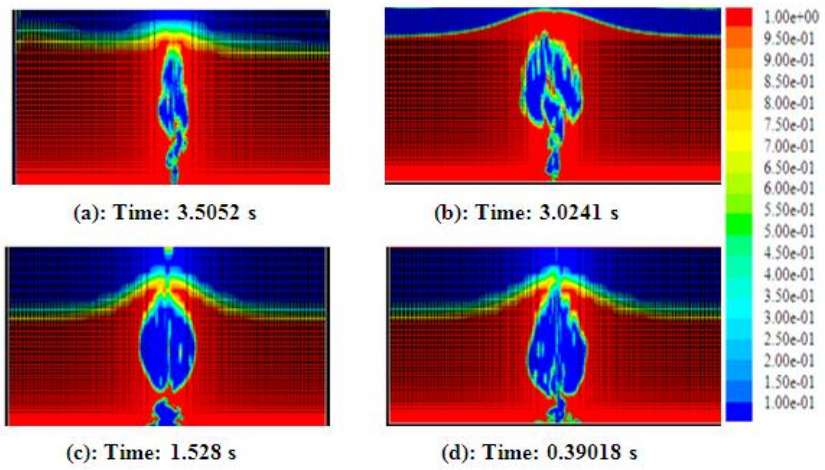

Fig. 4.3: Effect of varying hole diameter shown by contours with respect to primary phase.

Depth: 300 m; **Hole diameter:** (a) 20 mm, (b) 30 mm, (c) 50 mm, (d) 100 mm

The larger the hole size, the less time the plume takes to reach the free water surface, and affects larger free surface.

For various hole diameters and depths the time taken to reach the free surface, plume width and fountain height for the plume release are shown in table 4. The plume width and the fountain height were calculated according to the number of cells in the grid.

Table 4: Data obtained for plume width and fountain height

Hole diameter (mm)	Depth taken for simulation (m)	Mass flow inlet (kg/s)	Time taken by plume to reach the free surface. (s)	Fountain height (m)	Plume width (m)
20	0.5	10	0.07036	0.5	< 2
20	1	9.963	1.0888	1.5	2
20	3	9	3.50525	0.5	2.5
20	4	9.55	6.9908	0.35	5
30	0.5	22.61	0.04088	1.25	2
30	1	22.41	0.30068	2	2.5
30	3	20.5	3.0214	1	3
30	4	21.5	4.66	< 1	6
50	1	62.27	0.1	1	2

50	3	56.95	1.5258	2.4	4
50	4	59.71	2.07	2	5
100	1	248	0.13003	> 2.5	2
100	3	227.7	0.39108	1.5	> 4
100	4	238.8	0.412	< 1.5	> 3

4.3 Boil-off condition

In order to study the effect of boil off the gas at various flow conditions a test was conducted with respect to pressure. Because of energy input via pumps, heat transfer takes place through the walls of the cryogenic pipe. Thus there is an increase in temperature of LNG up to about near boiling conditions. The conclusion from the test was that it may result in large deviation of pressure because this may lead to formation of gas in the hose. High LNG transfer rates are required for economical benefits resulting in considerable flow through the piping with velocity up to 10 m/s, while the usual flow velocities in processing liquids are typically in the range of 1 m/s - 4 m/s. As flow rate increases in the pipe turbulence is generated in the pipe, creating a gas during LNG transportation in pipes or hoses. This enhance the pressure loss across the pipe that may result into cavitations at downstream stages of the pipe.

Pipelines are very important and comparatively safe means of transport for fluids. In a case if accident occurs, consequences may be drastic. Due to different causes, pipeline undergoes loss of integrity which may lead to failure. In a worst case, the failure results in a burst that breaks the line. The mathematical problem to be solved for simulating outflow comprise the equation of mass, momentum and energy. According to rupture configuration, gas can interact with some obstacle and then spreads out in the ambient atmosphere. Modeling gas release is necessary in order to evaluate jet characteristics.

The correlations used for the calculation of release of LNG when it is in the gaseous form in the pipe, are given below:

$$CPR = \frac{P_b}{P_{acr}} = \left(\frac{2}{\gamma+1}\right)^{\frac{\gamma}{\gamma-1}} \quad (33)$$

When, $P_a < P_{acr}$

$$Q = C_o S_o P_a \sqrt{\frac{2M\gamma}{zRT_2(\gamma-1)}\left[\left(\frac{P_b}{P_a}\right)^{\frac{2}{\gamma}} - \left(\frac{P_b}{P_a}\right)^{\frac{\gamma+1}{\gamma}}\right]} \quad (34)$$

When, $P_a > P_{acr}$

$$Q = S_{or} P_a \sqrt{\frac{M\gamma}{zRT_2}\left(\frac{2}{\gamma+1}\right)^{\gamma+1/\gamma-1}} \quad (35)$$

The value of release rate from the orifice depends on the critical pressure ratio, CPR, which indictates whether the release will be sonic or sub-sonic. (Yuhu et al., 2003).

The mass flow rate calculated with these conditions results in higher mass flow rate, as compared to the earlier cases. This high release rate would result in more eruption and rises violently in the domain, and affects very large area of free surface. When gas is released with very high flow rate of 9 kg/s it would take about 0.24 s simulation time, and it rises very violently in the sea, resulting in higher fountain height, and wider plume width of about 5 m as compared to plume width of 1.5 m in case of release of lower mass flow for 20 mm diameter and a depth of 300 m. From the figures, it is also concluded that when the release occurs during the boil –off condition, it will take less time to reach the surface, as compared to other, and will affect free surface more violently.

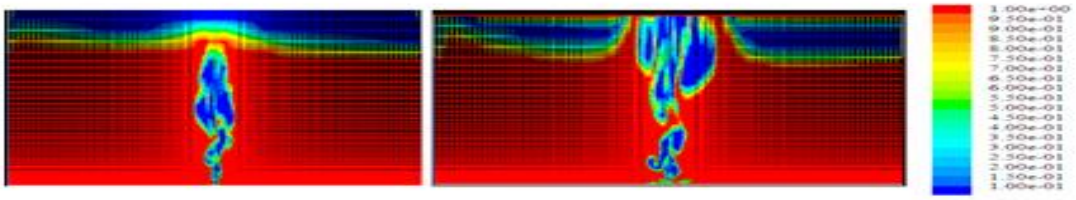

(a): Time: 3.505 s
Rate: 9 kg/s

(b): Time: 0.24 s
Rate: 305 kg/s

Fig. 4.4 Variation of mass flow rate Hole diameter: 20 mm Depth: 300m

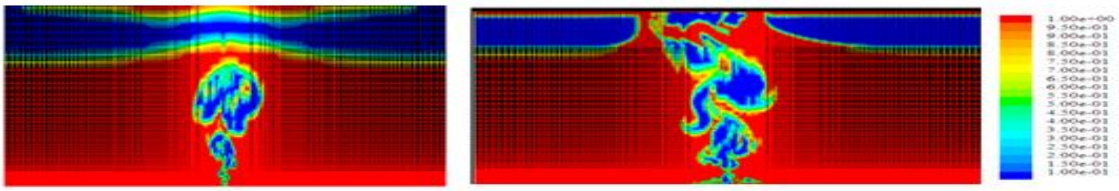

(a): Time: 4.66 s
Rate: 21 kg/s

(b): Time: 0.23 s
Rate: 687 kg/s

Fig. 4.5: Variation of mass flow rate Hole diameter: 30 mm Depth: 400 m

If the mass flow rate release keeps on increasing, then it would result in a very violent discharge and may spread in the environment, and can replace most of the air from the surface. From fig 4.5(b) and 4.6, one can see how destructively the plume rise and there by affect the large surface area.

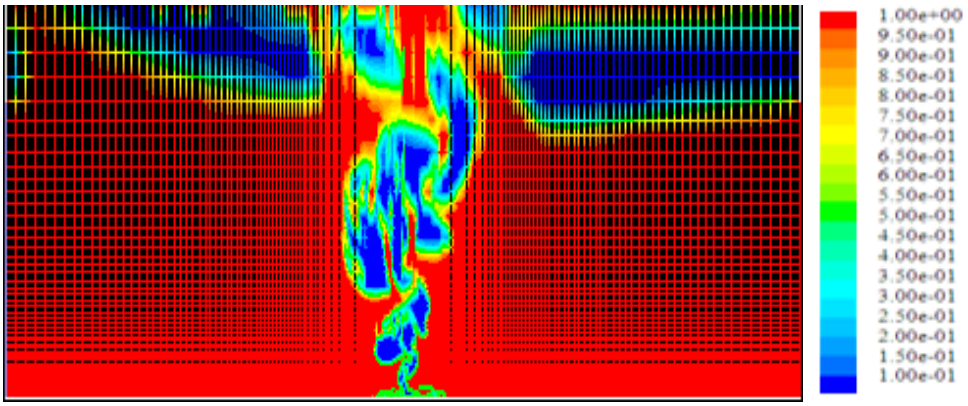

Fig. 4.6 Violent structure of sub-sea plume of mass flow rate 305 kg/s; Time: 0.24 s

Depth: 400 m; **Hole diameter:** 30 mm

As the gas is released from a hole in the pipe, the gas path velocity changes with height and time, as also, along the radial direction. The velocity of plume depends upon the hole size, water depth and mass flow rate of leak. Figs. 4.7 - 4.14 shows the instantaneous velocity changes.

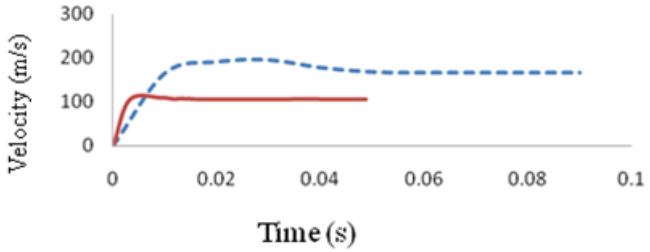

Fig.4.7: Velocity –Time plot

- - - - Hole size: 20 mm; **Depth:** 50; **Mass flow rate:** 10 kg/s

-----Hole size: 30 mm; **Depth:** 50; **Mass flow rate:** 22.61 kg/s

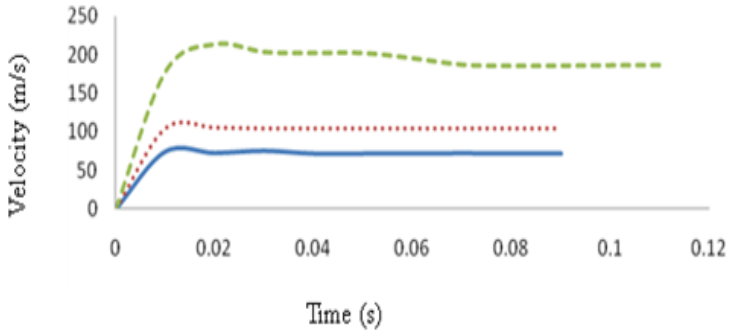

Fig.4.8 Velocity – Time plot

——Hole diameter: 20 mm; **Depth:** 100 m; **Mass flow rate:** 9.96 kg/s

·····Hole diameter: 30 mm; **Depth:** 100 m; **Mass flow rate:** 22.41 kg/ s

—·—Hole diameter: 20 mm; **Depth:** 100 m; **Mass flow rate:** 62.27 kg/s

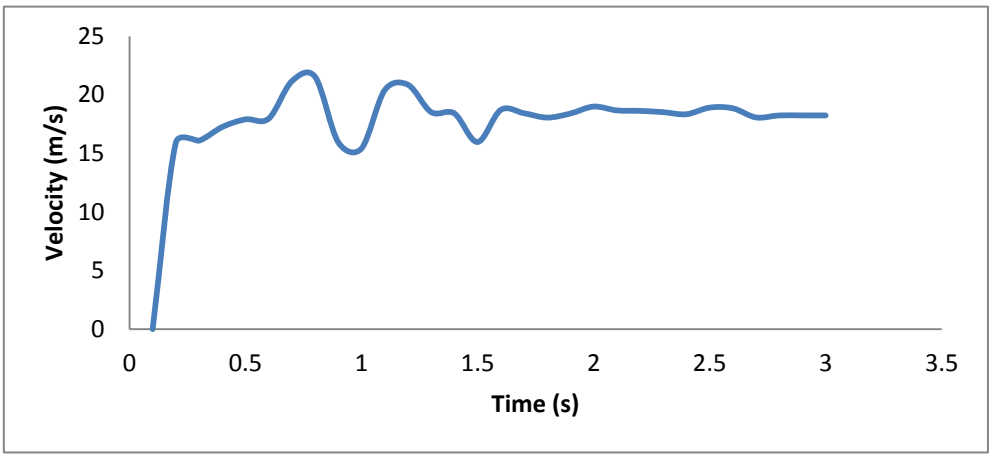

Fig.4.9: Velocity-Time plot

Hole size: 20 mm; **Depth:** 400 m; **Mass flow rate:** 9.55 kg/s

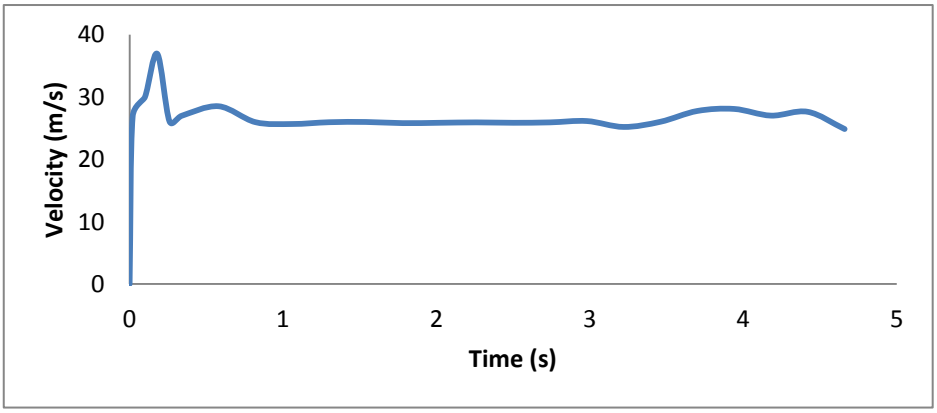

Fig.4.10: Velocity-Time plot

Hole size: 30 mm; **Depth:** 400 m; **Mass flow rate:** 21.5 kg/s

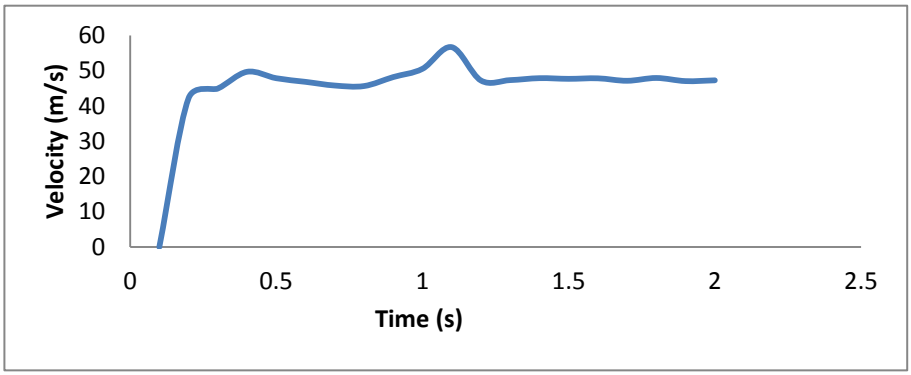

Fig.4.11 Velocity-Time plot

Hole size: 50 mm; **Depth:** 400 m; **Mass flow rate:** 59.71 kg/s

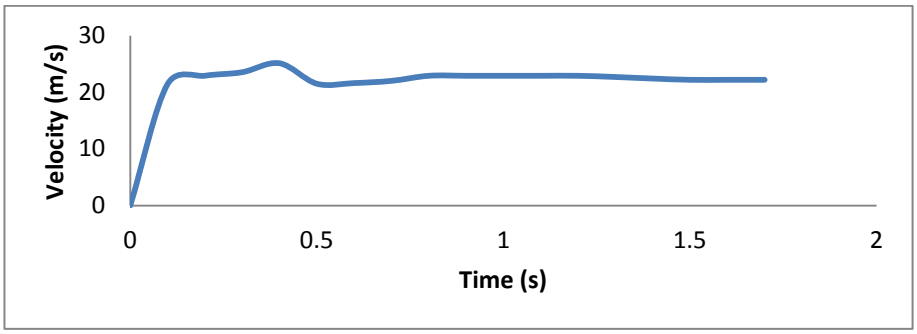

Fig.4.12 Velocity-Time plot

Hole size: 20 mm; **Depth:** 300m; **Mass flow rate:** 9 kg/s

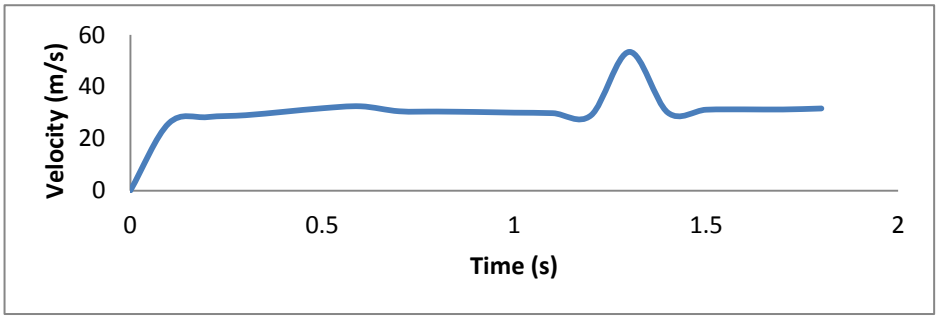

Fig.4.13 Velocity-Time plot

Hole size: 50 mm; **Depth:** 300 m; **Mass flow rate:**56 kg/s

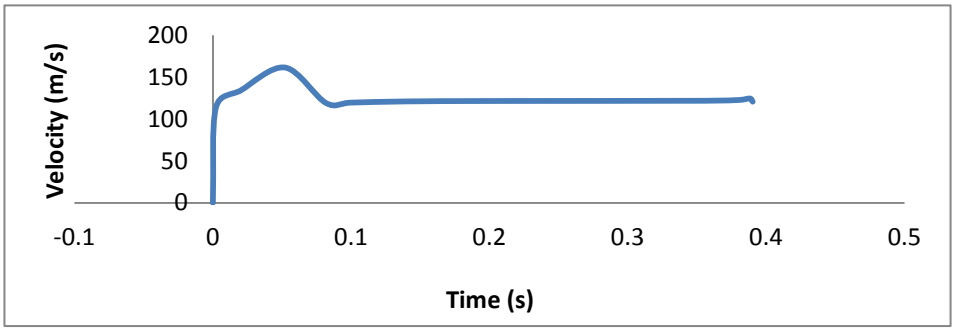

Fig.4.14 Velocity-Time plot

Hole size: 100 mm; **Depth:** 300 m; **Mass flow rate:** 227 kg/s

Similar trends for the velocity-time were shown by Cloete et al., (2009).

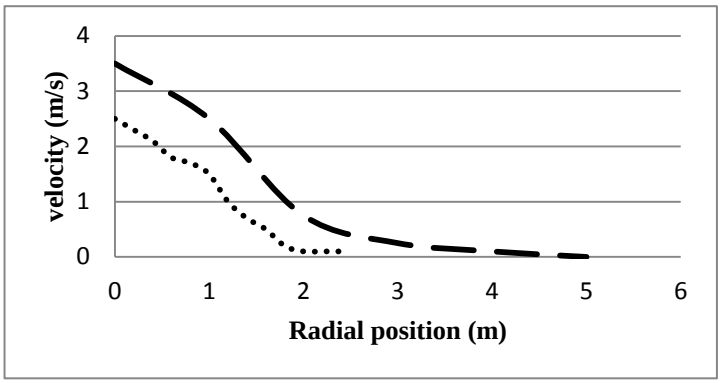

Fig. 4.15 Velocity profile vs Radial distance

…… Cloete et al., (2009) **Model:** 1.75 m; — — Simulated data;

Hole size: 30 mm; **Simulation depth:** 0.5 m

Fig. 4.15 shows the centerline velocity at radial position is, as obtained from the FLUENT simulator. The velocity – radial distance profile obtained by Cloete et al. (2009) is also similar. Similar curves were also obtained for other cases too, which are not plotted here as all are following similar trend.

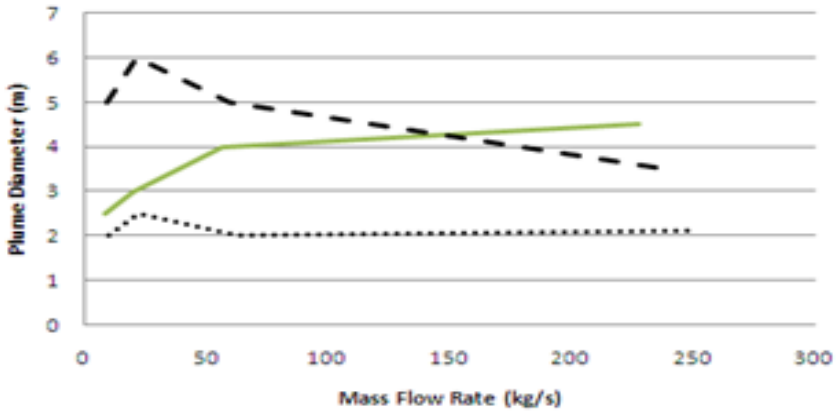

···· **Depth:** 100 m**; ——Depth:** 300 m**; — — Depth:** 400 m

Fig.4.16 Plume Diameter vs Mass Flow Rate

Fig 4.16 shows the plot of plume diameter for different mass flow rates. The mass flow rate varies with the hole diameter. From the above plot we can observe that at a given sea depth the

plume diameter increases with mass flow rate. For a depth of 400 m, the plume diameter increases first thereafter decreases because of the surface tension acting on the plume.

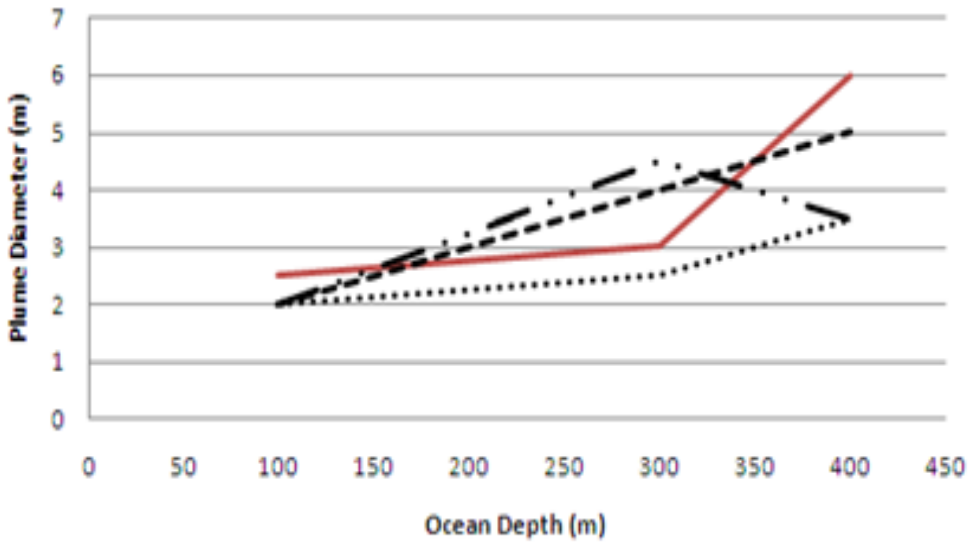

Fig. 4.17 Depth of water vs Plume Diameter

Hole diameter: ···· 20 mm; ——30 mm**;** — —50 mm; —··— 100 mm

As the gas is released from the pipe its initial pressure is high. Therefore, the gas expands, when it comes out of the pipe. The hydrostatic pressure acting on the plume decreases as the plume rises in the water column and allows the plume to diverge. Therefore, as the ocean depth increases, the plume diameter increases.

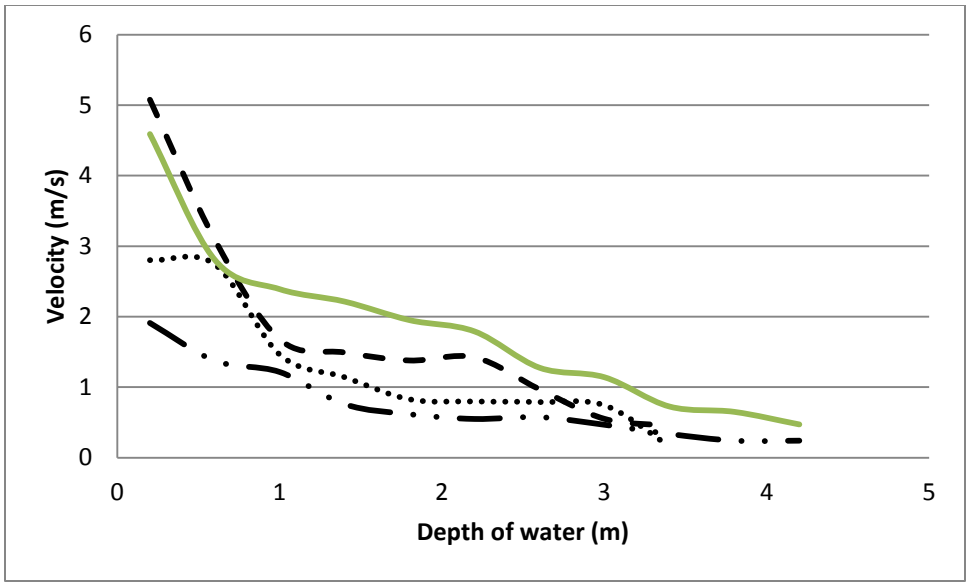

Fig. 4.18 Depth of Water vs Centerline velocity

···· **Hole diameter:** 20 mm**; Depth:** 300 m;— —**Hole diameter:** 30 mm**; Depth:** 300 m**;**

—· · —**Hole diameter:** 20 mm; **Depth:** 400 m——— **Hole diameter:** 30 mm**; Depth:** 400 m

As the depth of the water increases centre line velocity increases, this can be observed from the fig. 4.18.

4.4 Effect of water current

The effect of water current on the plume can be observed in Figs. 4.17 and 4.18. The separation of gas bubble from the main buoyant plume jet is seen in the ambient direction of cross-flow. The separation of bubbles will occur when horizontal ambient water will drive the entrained fluid away from the dispersed phase. These dispersed phases (gas bubbles) move with much higher velocity in axial direction than the fluid which is entrained, then bubbles move away from the main buoyant plume jet. As the gas bubble size is varied, we will have different rise velocity. Larger sized bubbles and droplets will be separated from the jet rapidly and move as individual bubble or droplet to the surface of water. The smaller sized bubbles will, however, continue to be moving moving within the main jet for a very long time. The trajectories of gas bubbles are affected by fractionation, which in turn affects the bubble distribution and location. When the bubbles are released from the pipe hole, these are modeled as a large number of individual particles using Lagrangian model. When these particles enter the computational domain through

a hole, random walk model is used to track them. As the gas particles or bubbles may get separated from the main plume jet during a cross flow, each particle motion has two states, the first state being within the plume and the other state being observed after the particle separation from the plume. (See Figs. 4.17 and 4.18)

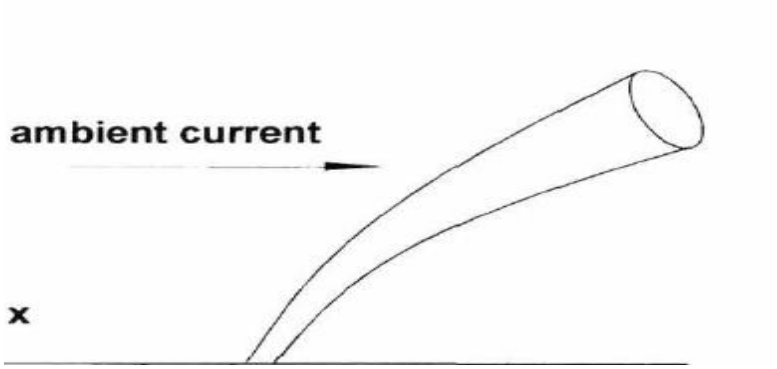

Fig. 4.19 Water-current profile for plume (Zheng and Yapa, 2002).

Figs 4.20 shows the simulation results for the release from a 20 mm hole at depth of 300 m (3m simulation depth) with a velocity of water current at 1 m/s, is shown. From this figure we can observe that the plume t shifts in the direction of the ambient current and ultimately reaches the surface, although after a long time. The simulation has run for about 1.38 s and the plume reached to a height of 1.5 m.

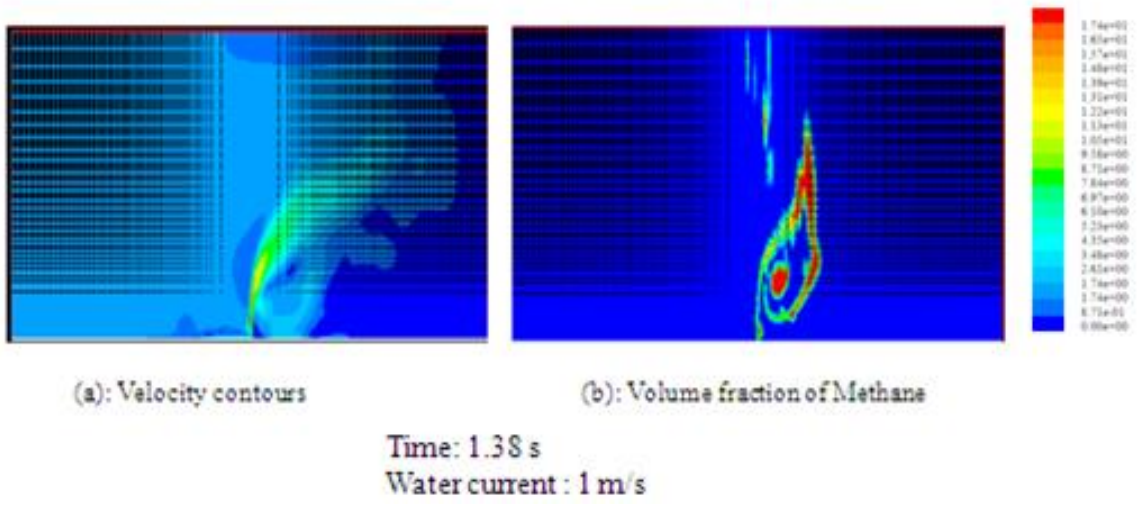

Fig.4.20 Effect of water current on LNG release

Hole diameter: 20 mm, Simulation depth: 3 m

After 5.66 s the plume will move further in the direction of water current. Fig 4.20 shows that the plume gets withered and gets converted into a large number of gas bubbles. Obviously, these bubbles will have a size distribution and therefore, the buoyant velocity distribution. This happens when the vertical velocity of the main plume carrying gas bubbles is reduced to its terminal velocity. Separated larger sized bubbles will reach up to the surface, and the smaller bubbles will travel a longer distance in water before they reach the water surface.

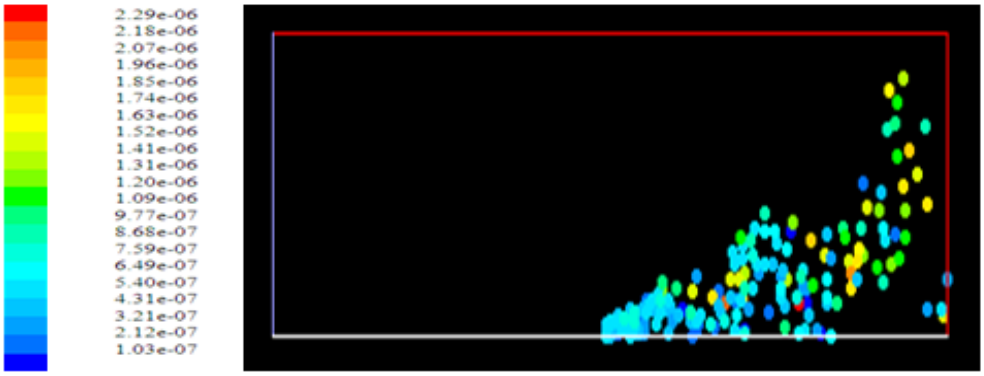

Fig.4.21 The effect of water current on plume behaviour

Time: 5.66 s; **Hole diameter:** 20 mm; **Depth:** 300 m (simulation depth: 3 m);

Mass flow rate: 22.41 kg/s

4.5 Effect of Temperature

As the gas is released underwater, it undergoes a rapid phase transition. Therefore, its temperature increases immediately. However, with the passage of time, the temperature starts decreasing. (ABS consulting, 2004).

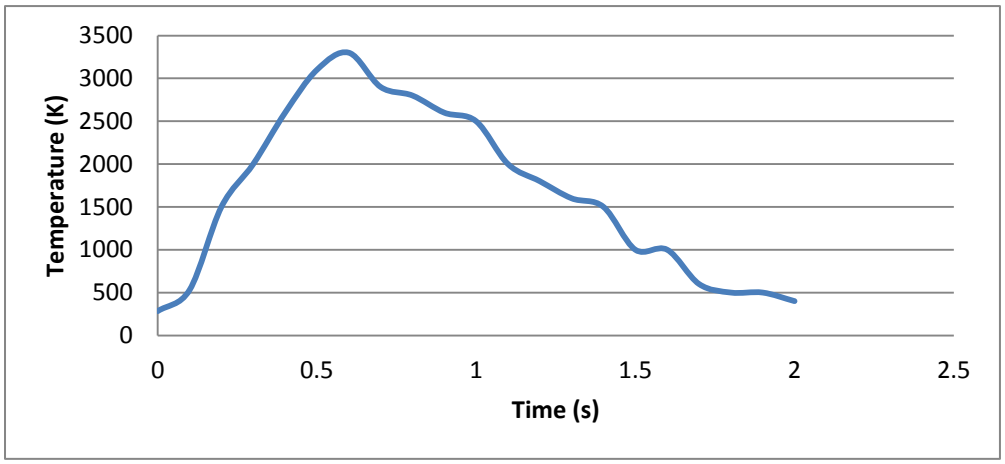

Fig.4.22 Temperature-Time profile

Fig.4.22 shows the temperature- time profile for a flow rate of 22.41 kg/s at 100 m depth (1 m simulation depth) for a hole size of 30 mm. It is seen that the temperature rises alarmingly upto ~3350 K and then decreases, ultimately reaching the saturation temperature of 190 K.

4.6 Concentration of methane in sea water

The concentration of methane in water changes with the depth of the sea. The methane concentration is more at near the release point but it decreases as it traverses to the surface. The methane concentration calculation can be performed through simulation, by using the DPM model. It is found that the concentration varies with the depth and with the number of bubbles. For a depth of 100 m (1 m simulation depth) and at a depth of 20 m (0.2 m simulation depth) was found to be 0.1965 kg/m^3. As the plume moves toward the free surface, the methane concentration was found to be 0.153 kg/m^3 at 50 m depth (0.5 m simulation depth) which then further reduced to 0.0642 kg/m^3 at 80 m depth. On the free water surface, the methane concentration was found to be 0.0123 kg/m^3. For the release from the hole of 30 mm and depth 50 m, the average concentration in the area of 2000 m^2(20 m^2 simulation area) was found to be 0.059 kg/m^3. In case of release of gas from a hole of 100 mm, at a depth of 400 m (simulation 4 m) the concentration at 200 m depth (2 m simulation depth) was found to be the 0.106 kg/m^3. These concentration illustrate the sum total of dissolved and free methane in water.

Response of toxic gas released underwater is noted down by seeing how fish responds to the dissolved or suspended toxicants. The effect of gas depends on the nature of the toxicant,

exposure time and environmental conditions. Researchers conducted experiments in the sea of Asov, after accidental gas blow out on drilling platforms during summer- autumn of 1982 and 1985. They found that the methane concentration near the release point was 4 x 10^{-3} - 6 x 10^{-3} kg/m^3, 7 x 10^{-5} – 1.4 x 10^{-3} kg/m^3 at a distance of 200 m and 3.5 x 10^{-3} kg/m^3 at a distance of 500 m. This shows that the methane can stay in environment for a long period. The presence of methane gas in water shows a olfactory sensitivity for fishes as studied by researchers to judge the behavioral response of the marine animals. The threshold value for such animals is found to be 1 x 10^{-4}- 5 x 10^{-4} kg/m^3 but if the concentration keeps on increasing this may lead to death of fishes. If the concentration reaches to 1 x 10^{-3} - 3 x 10^{-3} kg/m^3 then it would cause death of fishes within 48 h. Zooplankton dies when it get exposed to 5.5 x 10^{-3} kg/m^3 concentration of methane for 96 hours. This means that the fishes die sooner than the zooplankton. When the gas levels increase quickly then this may lead to the death of the marine animals quickly. (http://www.offshore-environment.com/gasimpact.html).

The methane concentrations as obtained from the simulation runs are very large than the threshold value for fishes/ zooplankton. Thus, these concentrations will lead to death of marine animals.

Methane concentration also varies with the radial position on the free surface, the lower concentration was observed for a depth of 400 m, because the gas dispersed in radial direction upon release, there by diluting the upward momentum of the gas.

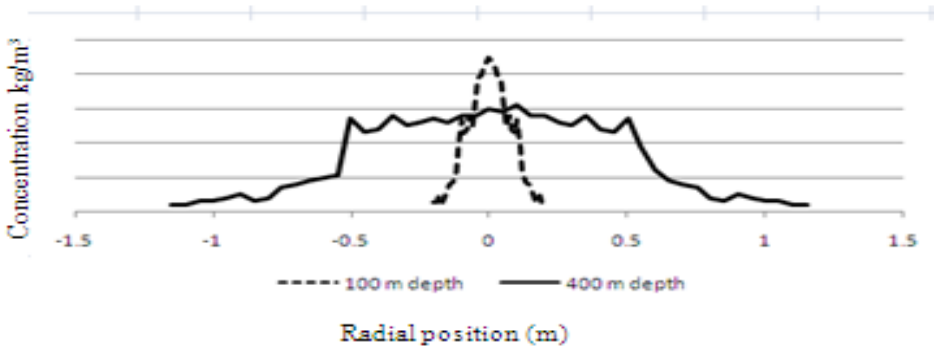

Fig.4.23 Concentration profile on free surface

Hole size: 20 mm; **Depth:** 100 m, 400 m

Fig. 4.20 shows the concentration profile of methane at 100 m and 400 m depth along the radial position from the center line of the plume. This plot is showing initial concentrations for the release from a hole of 20 mm at depth 100 m and 400 m.

In deep water, the behavior of gas is non-ideal due to high ambient pressure. Due to expansion and dissolution continually, there is a variation in gas bubbles size and shape significantly. While estimating the mass transfer coefficient and solubility of gas bubbles in water, these factors are needed to be considered. Gas solubility formulation is valid for high and low pressures. In general, the dissolution rate for a gas bubble is calculated by

$$\frac{dn}{dt} = KA(C_s - C_0) \tag{36}$$

C_o is concentration of dissolved gas (mol/m^3), and Cs is the saturated value of dissolved gas (i.e., solubility).

The solubility of gas in water is generally calculated by the simple Henry's Law:

$$P = Hx^1 \tag{37}$$

This law is limited to its application to low pressure condition gases or ideal gases. If the pressure is increased i.e., as we go in deep water, we have the modified form of Henry's law for the solubility of slightly soluble gases at very high pressures, (Zheng and Yapa, 2002).

$$f^g = Hx^1 \exp\left(\frac{10^6 P \vartheta^1}{RT}\right) \tag{38}$$

The coefficient of mass transfer of gas bubbles in liquids is a function of the shape and size of the bubbles as well as the diffusivity of gas the in liquids.

Generally gas bubbles in liquid are considered as sphere ideal particles for small sized bubbles, ellipsoids for intermediate sized bubbles, and spherical caps for larger sized bubbles.

For bubbles with spherical shape (small sized bubbles), the mass transfer coefficient is obtained from (Zheng and Yapa, 2002).

$$K = 0.0113\left(\frac{UD}{0.45+0.2d_e}\right)^{1/2} \qquad d_e < 5 \text{ mm} \tag{39}$$

Where, de is the equivalent diameter of the bubbles in cm, and D is the molecular diffusivity of gas in liquids (cm^2/s)

For bubbles considered with ellipsoidal shape (intermediate size bubble), the mass transfer coefficient is obtained from

$$K = 0.065D^{1/2} \qquad 5 \text{ mm} < d_e < 13 \text{ mm} \qquad (40)$$

Whereas, for bubbles considered as spherical cap shaped (large sized bubbles)

$$K = 0.0694 d_e^{-1/4} D^{1/2} \qquad d_e > 13 \text{ mm} \qquad (41)$$

Buwa, et al., (2006), and Cloete, et al.(2009), showed that the critical diameter of bubble for transition from intermediate size to large size bubbles should be taken as 5 mm.

Mass transfer coefficient was obtained by using the relation given for intermediate size and it was obtained to be 2.055×10^{-6} and the dissolution rate was obtained as 5.25×10^{-13}, which is very small. These calculations were made by using 5 mm bubble diameter. This shows that the methane gas dissolves in the sea water at a very slow rate, and hence it will take a long time to attain the toxicity level of the gas in water.

Table 5: LNG jet behavior in water column

depth (m)	**Hole size (mm)**	**Pressure of water (kPa)**	**Area of hole (m^2)**	**Vertical distance where jet breaks down (S_d)**	**Jet out flow velocity (m/s)**
50	20	500	3.14×10^{-4}	0.2	74.40
100	20	1000	3.14×10^{-4}	0.2	73.74
300	20	3000	3.14×10^{-4}	0.2	67.44
400	20	4000	3.14×10^{-4}	0.2	70.72
50	30	500	7.06×10^{-4}	0.3	74.40
100	30	1000	7.06×10^{-4}	0.3	73.74
300	30	3000	7.06×10^{-4}	0.3	67.44
400	30	4000	7.06×10^{-4}	0.3	70.72
50	50	500	1.96×10^{-3}	0.5	74.40
100	50	1000	1.96×10^{-3}	0.5	73.74
300	50	3000	1.96×10^{-3}	0.5	67.44
400	50	4000	1.96×10^{-3}	0.5	70.72
300	100	3000	7.85×10^{-3}	1	67.44

Using the correlations proposed by Raj and Bowdoin (2010), as described in chapter 3, calculations were made about the LNG jet behavior in water column. Table 5 shows that vertical distance where jet breaks down and the droplets forms and the liquid jet outflow velocity for different depths and hole diameters.

Table 6: Liquid Droplet diameter calculation

Depth (m)	**Hole diameter (mm)**	**Effective diameter (m)**	**d_p (m)**	**Velocity (m/s)**	**Surface tension (N/m)**
0.5	20	4.798×10^{-3}	0.000939	0.1260	0.0715
1	20	4.77×10^{-3}	0.001023	0.1315	0.0706
3	20	4.706×10^{-3}	0.001159	0.1400	0.0674
4	20	4.695×10^{-3}	0.001183	0.1415	0.0667
0.5	30	4.798×10^{-3}	0.000939	0.1260	0.0715
1	30	4.77×10^{-3}	0.001023	0.1315	0.0706
3	30	4.701×10^{-3}	0.001159	0.1400	0.0674
4	30	4.695×10^{-3}	0.001183	0.1415	0.0667
0.5	50	4.798×10^{-3}	0.000939	0.1260	0.0715
1	50	4.777×10^{-3}	0.001023	0.1315	0.0706
3	50	4.70×10^{-3}	0.001159	0.1400	0.0674
4	50	4.6953×10^{-3}	0.001183	0.1415	0.0667
3	100	4.701×10^{-3}	0.001159	0.140054	0.0674

The varying surface tension with depth, as calculated in the above table, was obtained by using the correlations and the data given by Sachs et al., (1995) and Schmidt et al., (2007). Time of evaporation for the largest droplet is calculated, this time of evaporation is a function of heat transfer coefficient which depends on the depth and temperature difference between the environmental temperature i.e., that of water and the saturated temperature of the gas. Table 7

shows that the superheated liquid droplet which will become unstable due to rapid superheating, resulting in violent superheat loss and phase change activity. This results in rapid release of vapor bubbles and creates strong shockwaves.

Table 7. Heat transfer effect on Liquid Droplets.

Heat transfer coefficient (W/m^2K)	**Excess temperature (k)**	**Viscosity (Pa.s)**	**Depth (m)**	**Thermal conductivity**	**Time of evaporation (s)**	**Vertical distance (m)**
144.4410028	164	1.6366×10^{-5}	400	0.03163	5.47804	0.25844
144.8292	166	1.6472×10^{-5}	300	0.031912	5.285	0.2467
145.2267	168	1.6576×10^{-3}	100	0.032196	4.5959	0.2015
145.6250	170	1.668×10^{-5}	50	0.03248	4.1577	0.1747

From the above table the distance where the jet gets completely breakdown into droplets, and how long these droplets will reside in water are obtained. The diameter of the largest droplet was determined, which gets disintegrated into bubbles after some time due to thermal instability. This thermal instability was obtained by calculating the time of evaporation of the droplets. The droplets also travel some distance in the upward direction after which they break down into bubbles. The time of evaporation of the droplets depends on the heat transfer coefficient which is a function of the surface tension, which in turn depends on the depth of the sea.

Chapter 5

Conclusions and Recommendations

5.1 Conclusions

A comparative study is done among three models that is Empirical Model, Integral Model and CFD model to study about the release of LNG/NG from the leakage points in a pipe lying underwater of different depth.

The release of gas in the deep-sea represents a hazardous situation. A CFD calculation has been performed in simulating the methane (major constituent of LNG) concentrations and its spread in water. The sudden burst of gas results in a quasi-steady flow, the gas plume which results in a starting plume, appears like a spherical cap shaped plume rising from leakage point. Turbulence and lift forces supplies lateral force to radially spreading of the bubbles but have very little effect on velocity components. If these forces are not involved in the two-phase equations, no spreading of plume occurs and the characteristic Gaussian shape would not be reproduced. This cryogenic liquid jet which is release under water would result in rapid shattering of mushroom like structure into small liquid droplets that are order of tens of centimeter to meter. The total amount of thermal energy of methane is almost the same when pipeline operating pressure (pipeline pressure larger than critical pressure) and hole size are same.

Simulations were carried out at various depth of 50 m, 100 m, 300 m, 400 m for different hole diameters 20 mm, 30 mm, 50 mm, 100 mm, the large amount of gas volume is present in the bubble which rises. The gas concentration in the atmosphere after the release LNG will be of interest in safety studies. Plume width and fountain height were seen through which one can predict how much area will be needed for safety consideration.

The concentration of methane in water was found to be more than the threshold limit for fishes. The high concentration of methane results in the death of marine animals.

6.2 Recommendations

1. When the gas is released under water it rises in the form of bubbles so the number of bubbles rising and reaching the surface should be explored.
2. Effect of temperature on the rising bubbles, how the bubble size and their movement due to buoyancy is affected by high temperature, because of release of the gas needs further study.
3. Study can also be done for the leak structure from the gas- drilling site in a porous rocky where gas drilled from the rocky structure.

References

- ABS Consulting. 2004. Consequence Assessment Methods for Incidents Involving Releases from Liquefied Natural Gas Carriers.
- Bettelini, M.S.G., Fannelop .T.K. 1993.Underwater plume from an instantaneously started source. Applied Ocean Research 15, 195-206.
- Billeter, L, Fannelop, T.K. 1989, Gas concentration over an underwater gas release. Atmospheric Environment 23, 1683-1694.
- Buwa, V.V, Deo, S.D, Ranade, V.V. 2006. Eulerian-Lagrangian simulations of unsteady gas- liquid flows in bubble columns. International Journal of Multiphase Flow 32, 864-885.
- Chahed, J, Roig, V, Masbernat, L. 2002. Eulerian–Eulerian two-fluid model for turbulent gas–liquid bubbly flows. International Journal of Multiphase Flow 29, 23-49.
- Cleaver, R.P., Cumber, P.S., Genillon. 2001. A Model to Predict the Characteristic of Fires Following the Rupture of Natural Gas Transmission Pipelines. Institution of Chemical Engineers Trans Institution of Chemical Engineer 79.
- Cloete, S., Olsen, J.E., Skjetne, P. 2009. CFD modeling of plume and free surface behavior resulting from a sub-sea gas release. Applied Ocean Research 31, 220-261.
- Cloete, S.W.P, Eksteen, J.J, Bradshaw, SM. 2009. A mathematical modeling study of fluid flow and mixing in full scale gas stirred ladles. M.S Thesis 1-261.
- Dhotre, M.T, Smith. B.L. 2007.CFD simulation of large-scale bubble plumes: Comparisons against experiments. Chemical Engineering Science 6, 6615-6630.
- Donald, L.K., Cornell, D., Kobayashi, R., Vary J.A., Elenbaas J.R., Weinaug C.F., Poettmann F.H.1959. Handbook of Natural gas Engineering. Mc Graw-Hill Book Company,INC., NewYork Toronto London.
- Fannelop, T.K., Sjoen, K.1980. Hydrodynamics of underwater blowouts. Norwegian Maritime Research 4, 17 -34.
- Fannelop, T.K., Bettelini, M. 2007. Very Large Deep-Set Bubble Plumes From Broken Gas Pipelines. Report no. 6201. Engineering and Environmental Flow Analysis Asgardstrand.

- Hassan, A., Jassim Esam. 2013. Visulization and Measurement of Bubbly Two-phase Flow Structure Using Particle Imaging Velocimetry (PIV). 1st Annual International Interdisciplinary Conference, AIIC, Azores, Portugal, 24-26.
- Johanse, O., Henrik, R.,Cortis, C. 2003. DeepSpill—Field Study of a Simulated Oil and Gas Blowout in Deep Water. Spill Science & Technology Bulletin 8, 433–443.
- Kobus, H.E. 1968. Analysis of the flow induced by air-bubble systems. In Proc. Coastal Engng Conf. London 11, 1016-1031.
- Kimme A., 2006. Pressure Induced Non-Linear Oscillations in two-phase LNG pipe flow. 6th Topical conference on Natural gas utilization Orlando, Florida.
- Kumar, S., Hyouk, T., Kwang, H.C., JaeHyunCho, WonsubLi, IlMoona, 2011. Current status and future projections of LNG demand and supplies: A global prospective. Energy Policy 39, 4097-4104.
- Lin, W., Zhang, N., Anzhong, G. 2010. LNG (Liquefied Natural Gas): A necessary part in China's future energy infrastructure. Energy 35, 4383–4391.
- Loes, M., Fannelop, T.K., 1989. Concentration measurements above an underwater release of natural gas, SPE Drilling, 171-178.
- McDouqal, T.L.J. 1978. Bubble plumes in stratified environments. Journal of Fluid Mechanics 85, 665-672.
- Milgram, J.H., Burgess, J.J. 1984. Measurement of surface flow above round bubble plume. Applied Ocean Engineering 6, 40-44.
- Milgram, J.H., Van Houten, R.J. 1982. Plumes from subsea well blowouts. Proceedings of 3rd Tnt. Conf. BOSS 1, 659-684.
- Milgram, J.H., 1983. Mean flow in round bubble plumes. Journal of Fluid Mechanics 133, 345-376.
- OGP draft 116903, Characteristic of LNG, influencing the design and material section. 2012.(https://www.google.co.in/url?sa=t&rct=j&q=&esrc=s&source=web&cd=2&cad=rja&ved=0CDAQFjAB&url=http%3A%2F%2Fwww.ogp.org.uk%2Findex.php%2Fdownload_file%2Fview%2F321%2F2876%2F&ei=pA1FUt73B4eyrAfEhYDoCA&usg=AFQjCNFaErtXftE6AuuyxMN8SNDo932xRA&sig2=M39ZDzkl4Q3hvva9qU1eQ&bvm=bv.53217764,d.bmk)

- Peng D.Y., Robinson D.B. 1976. A New Two-Constant Equation of State. Industrial and Engineering Chemistry Fundamental 15, 59-64.
- Ping, L.I., XueWei, L.I.U., LiMin, G.O.U., XiangChun, W.A.N.G., JunJie, Y.I.N., ChengLiang, X.I.N. 2013. Numerical simulation of bubble plumes in overlying water of gas hydrate in cold seepage active region. Science China, Earth Science 56, 579-587.
- Qi, R., Raj, P.K., Mannan, M., 2011. Underwater LNG release test findings: Experimental data and model results. Journal of Loss Prevention in the Process Industries 24, 440-448.
- Qi, R., Raj, P.K., Mannan, M., 2010, Numerical Simulations of LNG vapor Dispersion in Brayton Fire Training Field tests with ANSYS CFX. Journal of Hazardous Material 183, 51-61.
- Rew, P.J, Gallagher, P, Deaves, D.M. 1995. Dispersion of Subsea Releases-Review of Prediction Methodology. Health and Safety Executive- Offshore Technology Report OTH 95465.
- Rensen, J., Roig, V, 2001. Experimental study of unsteady structure of a confined bubble plume. International journal of Multiphase flow 27, 1431-1449.
- Sachs, W., Meyn, V. 1995. Pressure and temperature dependence of the surface tension in the system natural gas/water Principles of investigation and the first precise experimental data for pure methane/water at 25^0C up to 46.8 MPa. Colloids and Surfaces 94, 291-301.
- Schmidt, K.A.G., Folas, K.G., Kvamme, B.2007. Calculation of the interfacial tension of the methane–water system with the linear gradient theory. Fluid Phase Equilibria 261, 230-237.
- SINTEF. 2009. Assessing Risk and Modeling a Sudden Gas Release Due to Gas Pipeline Ruptures. US department of interior Minerals Management Service. Trondheim, Norway and Wellflow Dynamics Oslo, Norway.
- Smith, B.L, 1998. On the Modelling of Bubble Plumes in a Liquid Pool. Applied Mathematical Modelling 22, 773-797.
- Spaulding, M.L., Bishnoi, P.R., Anderson, E., Isaji,T. 2000. An Integrated Model for Prediction of oil transport from a deep water blow out. Ocean Engineering, University of Rohde Island, Narragansett RI 02882.

- Sridher, 2011. Validating sub-sea gas pipeline leaks discharge models for Arabian sea Condition. University of Petroleum and Energy studies, Dehradun, India.
- Sworn, C., Moros, A. 1993. Hydrodynamics of sub-sea blow out. Applied Ocean Research 15, 269-280.
- Topham, D.R., 1984. The formation of gas hydrates on bubbles of hydrocarbon gases rising in sea water. Chemical Eng. Science 39, 821-828.
- Xuegang, L., Hongchao, J., Yaogang, L. 2012. FLUENT in the Simulation of the Application of the Natural Gas. Proceedings of 2012 International Conference on Mechanical Engineering and Material Science.
- Zheng, L., Yapa. P.D. 2002. Modeling Gas Dissolution in Deep water oil/gas Spills. Journal of Marine Systems 31, 299-309.
- http://worldoceanreview.com/en/wor-1/ocean-chemistry/climate-change-and-methane-hydrates/2/.
- http://total.com/en/energies-expertise/oil-gas/trading-shipping/fields-of-expertise/transportation-storage/gas-pipelines.
- http://www.specialpiping.com.au/lng.html
- http://www.eia.gov/pub/oil_gas/natural_gas/analysis_publications/ngpipeline/process.html
- http://www.energy.siemens.com/hq/en/industries-utilities/oil-gas/applications/gas-liquid-pipeline.htm
- http://www.pipelineandgasjournal.com/velocity-midstream-signs-deal-gardendale-pipeline-terminal
- http://www.gastechnews.com/uncategorized/impact-of-boil-off-gas-in-lng-transfer/
- http://www.aga.org/Kc/aboutnaturalgas/consumerinfo/Pages/NGDeliverySystem.aspx
- http://www.jmcampbell.com/tip-of-the-month/2012/09/low-pressure-versus-high-pressure-dense-phase-natural-gas-pipeline-transportation/
- http://www.offshore-environment.com/naturalgas.html

Appendix

User Defined Functions

UDF's were used to reduce the pressure in the VOF simulation of bubble plume. The source code affecting the pressure reduction in the domain.

For 400m depth

```
#include"udf.h"
DEFINE_PROFILE(Pressure_magnitude,thread,position)
{
        real t;
        face_t f;
        t = CURRENT_TIME;
        begin_f_loop(f,thread)
        {
                F_PROFILE(f,thread,position)= 4000000-1000000*t;
        }
        end_f_loop(f,thread)
```

For 300m depth

```
#include"udf.h"
DEFINE_PROFILE(Pressure_magnitude,thread,position)
{
        real t;
        face_t f;
        t = CURRENT_TIME;
        begin_f_loop(f,thread)
        {
                F_PROFILE(f,thread,position)= 3000000-1000000*t;
        }
```

```
    end_f_loop(f,thread)
```

For 100m depth

```
#include"udf.h"
DEFINE_PROFILE (Pressure_magnitude,thread,position)
{
    real t;
    face_t f;
    t = CURRENT_TIME;
    begin_f_loop(f,thread)
    {
        F_PROFILE(f,thread,position)= 4000000-1000000*t;
    }
    end_f_loop(f,thread)
```

For 50 m depth

```
#include"udf.h"
DEFINE_PROFILE(Pressure_magnitude,thread,position)
{
    real t;
    face_t f;
    t = CURRENT_TIME;
    begin_f_loop(f,thread)
    {
        F_PROFILE(f,thread,position)= 500000-1000000*t;
    }
    end_f_loop(f,thread)
```

The UDF is compiled and then selected in inlet boundary condition panel.